Essential and unique roles of PIP5K-γ and -α in Fcγ receptor-mediated phagocytosis

Yuntao S. Mao,[1] Masaki Yamaga,[1] Xiaohui Zhu,[1] Yongjie Wei,[1] Hui-Qiao Sun,[1] Jing Wang,[1] Mia Yun,[4] Yanfeng Wang,[5] Gilbert Di Paolo,[6] Michael Bennett,[2] Ira Mellman,[4] Charles S. Abrams,[5] Pietro De Camilli,[7] Christopher Y. Lu,[3] and Helen L. Yin[1]

[1]Department of Physiology, [2]Department of Pathology, and [3]Department of Internal Medicine, University of Texas Southwestern Medical Center, Dallas, TX 75390
[4]Genentech Inc., South San Francisco, CA 94080
[5]Department of Medicine, University of Pennsylvania, PA 19104
[6]Department of Pathology and Cell Biology, Columbia University, New York, NY 10032
[7]Howard Hughes Medical Institute and Department of Cell Biology, Yale University, New Haven, CT 06520

The actin cytoskeleton is dynamically remodeled during Fcγ receptor (FcγR)-mediated phagocytosis in a phosphatidylinositol (4,5)-bisphosphate (PIP_2)-dependent manner. We investigated the role of type I phosphatidylinositol 4-phosphate 5-kinase (PIP5K) γ and α isoforms, which synthesize PIP_2, during phagocytosis. *PIP5K*-γ−/− bone marrow–derived macrophages (BMM) have a highly polymerized actin cytoskeleton and are defective in attachment to IgG-opsonized particles and FcγR clustering. Delivery of exogenous PIP_2 rescued these defects. PIP5K-γ knockout BMM also have more RhoA and less Rac1 activation, and pharmacological manipulations establish that they contribute to the abnormal phenotype. Likewise, depletion of PIP5K-γ by RNA interference inhibits particle attachment. In contrast, PIP5K-α knockout or silencing has no effect on attachment but inhibits ingestion by decreasing Wiskott-Aldrich syndrome protein activation, and hence actin polymerization, in the nascent phagocytic cup. In addition, PIP5K-γ but not PIP5K-α is transiently activated by spleen tyrosine kinase–mediated phosphorylation. We propose that PIP5K-γ acts upstream of Rac/Rho and that the differential regulation of PIP5K-γ and -α allows them to work in tandem to modulate the actin cytoskeleton during the attachment and ingestion phases of phagocytosis.

Introduction

Fcγ receptor (FcγR)-mediated phagocytosis is critically important for innate host defense, inflammation, and tissue remodeling (Groves et al., 2008). Professional phagocytes such as macrophages express FcγR to rapidly internalize opsonized pathogens and immune complexes (IC; Nimmerjahn and Ravetch, 2008). Phagocytosis involves spatially and temporally regulated steps including particle attachment, engulfment, and phagosome maturation (Groves et al., 2008). Actin assembles at the nascent phagocytic cup and during cup extension, and it disassembles during the completion of internalization (Swanson, 2008). Like actin, the phosphatidylinositol (4,5)-bisphosphate (PIP_2) level increases locally in the cup during ingestion and decreases before engulfment (Botelho et al., 2000). The current paradigm is that PIP_2 synthesis promotes de novo actin polymerization to initiate particle ingestion, whereas PIP_2 elimination depolymerizes actin to promote closure of the phagocytic cup (Yeung et al., 2006). Almost nothing is known about the role of PIP_2 and actin in the attachment phase.

Because phagocytosis invokes temporally defined steps that are spatially confined to the phagocytic cup, it provides an exquisite model to examine the molecular mechanisms by which PIP_2 synthesis and dissipation are regulated within this restricted membrane structure (Corbett-Nelson et al., 2006). PIP_2 is synthesized primarily by the type I phosphatidylinositol

Y.S. Mao and M. Yamaga contributed equally to this paper.

Correspondence to Helen L. Yin: helen.yin@utsouthwestern.edu

Abbreviations used in this paper: BMM, bone marrow–derived macrophages; C3T, C3 transferase; DIC, differential interference contrast; DN, dominant negative; ERK, extracellular signal-regulated kinase; FcγR, Fcγ receptor; HPLC, high-pressure liquid chromatography; IC, immune complexes; Jasp, jasplakinolide; Latr B, latrunculin B; PIP_2, phosphatidylinositol (4,5)-bisphosphate; PIP5K, type I phosphatidylinositol 4-phosphate 5-kinase; PV, pervanadate; Syk, spleen tyrosine kinase; TLC, thin layer chromatography; WASP, Wiskott-Aldrich syndrome protein; WT, wild type.

The Rockefeller University Press $30.00
J. Cell Biol. Vol. 184 No. 2 281–296
www.jcb.org/cgi/doi/10.1083/jcb.200806121

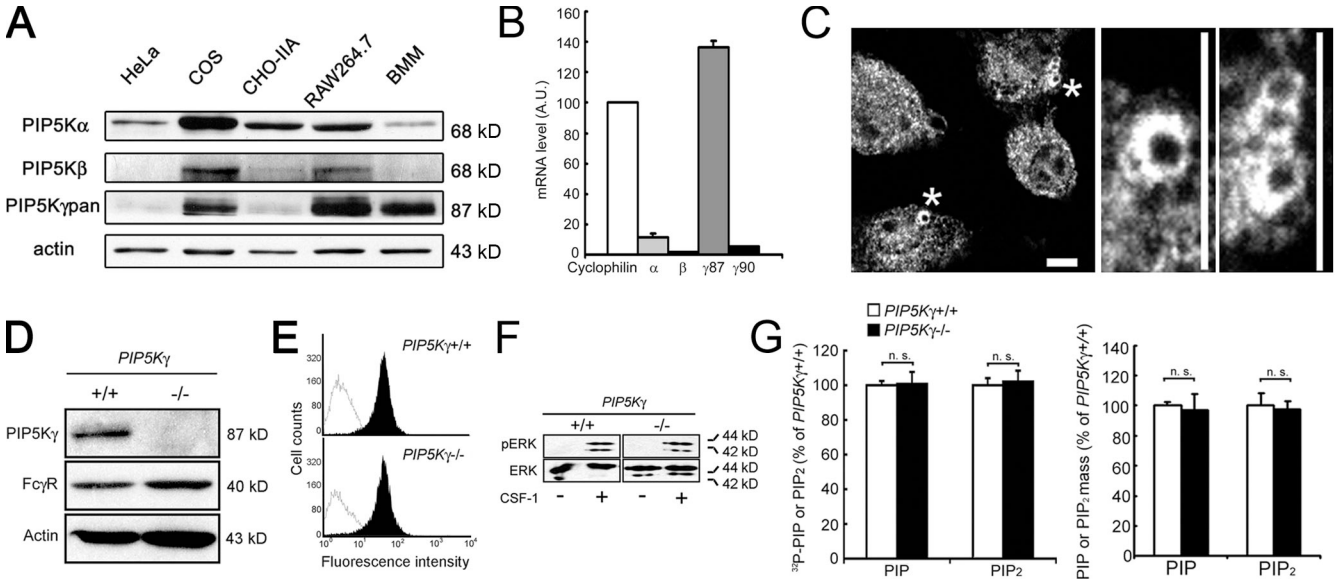

Figure 1. **Characterization of *PIP5K*-γ in BMM.** (A) Western blot of endogenous proteins in WT BMM. (B) Quantitative RT-PCR. The PIP5K level in WT BMM was normalized against cyclophilin (n = 3). (C) Recruitment of PIP5K-γ to the phagocytic cup. WT BMM exposed to IgG-opsonized particles were stained with anti–PIP5K-γpan antibody. The middle and right panels show enlarged views of regions marked by asterisks. Bars, 10 µm. (D) Western blot of *PIP5K*-γ−/− BMM. (E) FACs analysis of surface accessible FcγR. Black peaks, surface FcγR fluorescence; white peak, background. (F) CSF-1–induced ERK activation. CSF-1–stimulated BMM were extracted for Western blotting with anti-ERK and -pERK. (G) Phosphoinositide analyses. The PIP_2 or PIP value in *PIP5K*-γ−/− BMM was expressed as the percentage of WT cells. Left, TLC (n = 3). Right, HPLC (n = 4). Error bars indicate SEM. n.s., not significant.

4-phosphate 5-kinases (PIP5Ks), and mammals have three isoforms named α, β, and γ (for review see Mao and Yin, 2007). PIP5K-γ has several splice variants (Ishihara et al., 1998), and the two major variants, γ87 and γ90, are functionally distinct; PIP5K-γ87 supports PLCβ-mediated Ca^{2+} signaling in HeLa cells (Wang et al., 2004), whereas PIP5K-γ90 is implicated in synaptic transmission, endocytosis, and formation of focal adhesions (Di Paolo et al., 2002, 2004; Ling et al., 2002; Nakano-Kobayashi et al., 2007; Wang et al., 2007). There is emerging evidence from PIP5K RNAi (Padron et al., 2003; Wang et al., 2004; Micucci et al., 2008) and gene knockout (Di Paolo et al., 2004; Sasaki et al., 2005; Wang et al., 2007, 2008a,b) that the three PIP5K isoforms have unique roles in a tissue-specific manner. PIP5K-α (human isoform designation) has been implicated in FcγR-mediated phagocytosis (Coppolino et al., 2002), but the role of the other PIP5Ks has not been examined. Here, we show that PIP5K-γ and -α are both recruited to the phagocytic cup but that they regulate different steps in phagocytosis. PIP5K-γ promotes particle attachment by inducing controlled actin depolymerization to facilitate FcγR microclustering, whereas PIP5K-α promotes particle ingestion by activating the Wiskott-Aldrich syndrome protein (WASP) to induce Arp2/3-dependent actin polymerization at the nascent phagocytic cup. In addition, we show that PIP5K-γ is rapidly and transiently activated by the spleen tyrosine kinase (Syk), whereas PIP5K-α is not. Our findings establish that PIP5K-γ and -α orchestrate different types of actin remodeling at sequential stages of phagocytosis. They also suggest that PIP5K-γ tyrosine phosphorylation initiates actin depolymerization to promote FcγR microclustering during particle attachment and that it is tuned down to switch to net actin polymerization during the PIP5K-α–mediated ingestion step.

Results

Bone marrow–derived macrophages (BMM) have PIP5K-α and abundant PIP5K-γ87

Western blotting was used to compare the expression level of PIP5Ks in BMM with other types of cells. BMM had abundant PIP5K-γ, some PIP5K-α, and almost no detectible PIP5K-β (Fig. 1 A). The RAW264.7 macrophage-like cell line and nonmyeloid COS cells also had abundant PIP5K-γ, and more PIP5K-α and -β than BMM. In contrast, HeLa and CHO-IIA cells had more PIP5K-α and less PIP5K-β and -γ. We did not detect the γ90 variant in BMM even though it should be recognized by the anti–PIP5K-γpan antibody used (Wenk et al., 2001). PIP5K-γ90's low abundance was confirmed by the lack of staining with another antibody directed against PIP5K-γ90's unique C-terminal extension (unpublished data; Wenk et al., 2001).

Quantitative RT-PCR showed that PIP5K-γ87 was most abundant at the mRNA level in BMM compared with the other isoforms (Fig. 1 B), which corroborates the Western blot results. PIP5K-γ90 and β mRNA were ∼4% and 1% of PIP5K-γ87, respectively. In this paper, we used gene knockout and RNAi to examine the roles of PIP5K-γ and -α during FcγR-mediated phagocytosis.

PIP5K-γ−/− bone marrow precursor cells differentiate into BMM

Immunofluorescence labeling with anti–PIP5K-γpan showed that PIP5K-γ, which was predominantly cytosolic, was recruited to the nascent phagocytic cup during FcγR-mediated phagocytosis (Fig. 1 C). We used PIP5K-γ knockout to examine its role in BMM. Because *PIP5K*-γ−/− mice die within a day of birth (Di Paolo et al., 2004), their hematopoietic precursor cells were

transplanted into lethally irradiated wild type (WT) adult mice to generate sufficient *PIP5K*-γ−/− cells for experimentation. *PIP5K*-γ+/+ cells from pups from the same litter were transplanted in parallel to generate matched *PIP5K*-γ+/+ chimeras (WT controls). Reconstitution in the chimeras was established by flow cytometry to be 86–99% (Fig. S1 A, available at http://www.jcb.org/cgi/content/full/jcb.200806121/DC1). Western blotting confirmed that the *PIP5K*-γ−/− chimeric mice's BMM had no detectible PIP5K-γ (Fig. 1 D). Nevertheless, they expressed a normal amount of FcγR, as assayed by Western blotting with the 2.4G2 antibody that detects type II and III receptors (Fig. 1 D), and by FACs analyses of externally labeled FcγR (Fig. 1 E). In addition, like WT BMM (Wells et al., 2004), *PIP5K*-γ−/− BMM responded to colony stimulating factor-1 (CSF-1), a major macrophage growth and chemotactic factor, by robustly activating extracellular signal-regulated kinase (ERK; Fig. 1 F). Therefore, they are bona fide macrophages.

Although WT BMM have abundant PIP5K-γ, PIP5K-γ knockout had surprisingly little effect on ambient PIP_2 content, as assessed by thin layer chromatography (TLC), which depends on PIP_2 turnover, and by high-pressure liquid chromatography (HPLC), which measures lipid mass (Fig. 1 G). Western blotting did not detect a significant compensatory increase in PIP5K-α in BMM (Fig. S1B), which concurs with results from *PIP5K*-γ−/− brains (Di Paolo et al., 2004). Therefore, either PIP5K-γ is not a major contributor to BMM's ambient PIP_2 pool in spite of its relative high abundance, or its knockout induces compensatory changes in the activity of the other PIP5K isoforms or decreases overall PIP_2 turnover to maintain homeostasis.

PIP5K-γ−/− BMM have abnormal shapes and are defective in phagocytosis

WT BMM attached to coverslips were predominantly polygonal, whereas *PIP5K*-γ−/− BMM were often elongated and stellate (Fig. 2 A). *PIP5K*-γ−/− BMM also had brighter phalloidin staining, especially in the cell cortex. The bulk fluorometric phalloidin assay showed that there was a 50% increase in polymerized actin (Fig. 2 C). In addition, they phagocytized fewer IgG-opsonized particles (Fig. 2 A). Using incubation at 4°C versus 37°C to separate particle attachment (which can occur at 4°C) from engulfment (which does not occur at 4°C), we found that there was a marked decrease in particle binding (Fig. 2 A). The binding index (mean number of attached particles per cell) decreased by 70%, and the binding histogram shifted to the left (Fig. 2 A). The decrease in particle attachment paralleled that of ingestion, which suggests that the primary defect resides in the initial attachment phase. Similar inhibition was observed using IgG-opsonized sheep red blood cells (unpublished data).

PIP5K-γ−/− BMM have impaired responses to IC

The early zipper hypothesis proposes that particle attachment is mediated by the progressive interaction of FcγR with IgG (Griffin and Silverstein, 1974). Recently, there is increasing evidence that receptor microclustering increases the avidity of the receptors for their ligands (Cox and Greenberg, 2001). FcγR, which contains an immunoreceptor tyrosine-based activation motif (ITAM) (Nimmerjahn and Ravetch, 2008), oligomerizes to form microclusters (Sobota et al., 2005). The role of actin in FcγR microclustering has not been examined. Here, we investigated the possibility that the *PIP5K*-γ−/− BMM's particle attachment defect is caused by impaired FcγR microclustering by a static and excessively polymerized actin cytoskeleton.

Heat-aggregated IC, which have been used extensively to ligate FcγR (Nimmerjahn and Ravetch, 2008), were used to directly induce FcγR clustering, and anti-IgG was used to detect the clusters (Fig. 2 B). In WT BMM, IC binding was detected after a 5-min incubation at 4°C. By 20 min, the clusters became larger. Quantification by ImageJ showed that, on average, there was a 4.5-fold increase in cluster size (Fig. 2 B). Similar results were obtained when FcγR were directly stained with 2.4G2 (Fig. S2, available at http://www.jcb.org/cgi/content/full/jcb.200806121/DC1). In contrast, although IgG bound FcγR in *PIP5K*-γ−/− BMM, the size of FcγR–IgG clusters did not increase substantially between 5 and 20 min (Fig. 2 B). Therefore, receptor microclustering is impeded in *PIP5K*-γ−/− BMM.

IC stimulation induced a 40% decrease in polymerized actin in WT BMM (Fig. 2 C), providing evidence that FcγR ligation triggers dynamic actin rearrangements. In contrast, *PIP5K*-γ−/− cells, which already had higher basal polymerized actin content, did not depolymerize their actin after IC stimulation (Fig. 2 C). Collectively, our results suggest that *PIP5K*-γ−/− BMM have a highly polymerized actin cytoskeleton that is static and impedes FcγR microclustering.

FcγR ligation activates multiple downstream signaling pathways, including activation of the MAPK cascade, hydrolysis of PIP_2 by PLCγ, and conversion of PIP_2 to PIP_3 by phosphatidylinositol 3 kinases (Cox and Greenberg, 2001; Nimmerjahn and Ravetch, 2008). IC stimulated ERK phosphorylation to a much lesser extent in *PIP5K*-γ−/− BMM than in WT cells (Fig. 2 D), and depleted the PIP_2 pool in knockout macrophages only (Fig. 2 E). Attenuation of robust signal amplification is consistent with reduced FcγR microclustering and not a defect in the downstream ERK signaling cascade per se, as *PIP5K*-γ−/− BMM phosphorylated ERK normally in response to CSF-1 (Fig. 1 F). The differential effects of IC on WT and the *PIP5K*-γ−/− BMM PIP_2 level can be explained as follows. Although IC stimulates PIP_2 hydrolysis by PLCγ and conversion to PIP_3 by phosphatidylinositol 3 kinases, the steady-state PIP_2 level in WT BMM does not decrease because the pool is rapidly replenished. *PIP5K*-γ−/− BMM could not refill the pool, as reflected in a 40% decrease in the amount of PIP_2 after IC stimulation. Additional experiments will be required to determine why loss of PIP5K-γ interfered with the normal ability of BMM to replenish the IC-depleted PIP_2 pool.

Rescue of *PIP5K*-γ−/− BMM's phenotypes

We performed "rescue" experiments to establish a cause-and-effect relation between depletion of the PIP5K-γ–generated PIP_2 pool and the aberrant *PIP5K*-γ−/− phenotypes. First, we attempted to rescue the abnormal cell shape and attenuated particle binding by "shuttling" PIP_2 into BMM (Ozaki et al., 2000; Wang et al., 2003). PIP_2 delivery corrected *PIP5K*-γ−/− BMM's actin cytoskeletal and morphological defects (Fig. 3 A) and restored their ability to bind particles (Fig. 3 B). The carrier

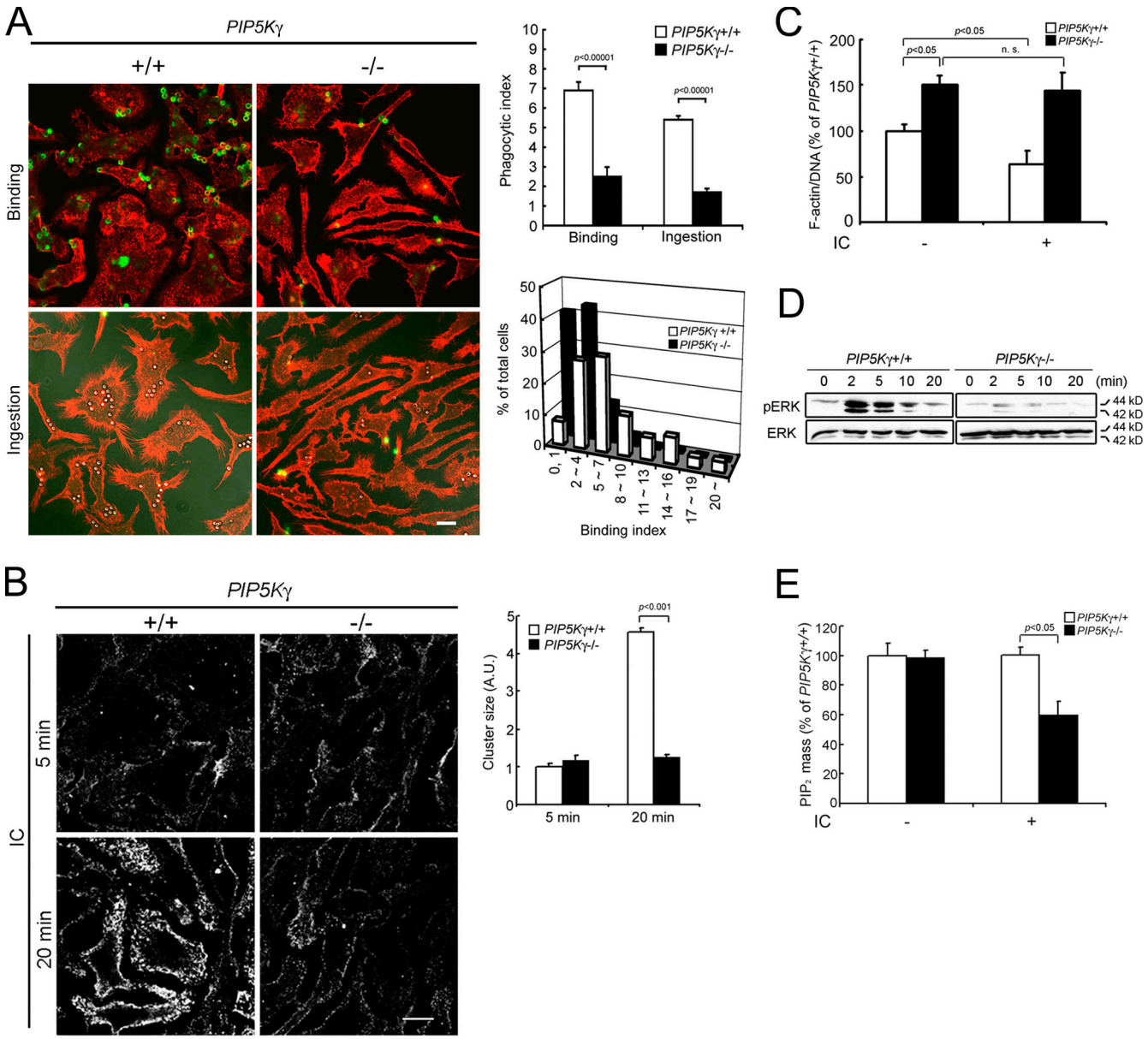

Figure 2. ***PIP5K*-γ−/− BMM are defective in attachment to IgG-opsonized particles and response to IC.** (A) Particle attachment and ingestion. (left) Fluorescence/DIC images. DIC images were overlaid on the fluorescence images in the "ingestion" panels. Green, external beads; red, phalloidin. (top right) Phagocytic indices, defined as the mean number of beads per cell (n > 150 cells). (bottom right) Particle attachment histogram. (B) IC-induced FcγR microclustering. BMM incubated with IC at 4°C were stained with anti-IgG to detect FcγR clusters on the cell surface. (left) Fluorescence images. (right) Cluster size quantitation by ImageJ (n = ~10,000 clusters). Size was expressed in arbitrary units (A.U.) relative to WT BMM at 5 min. Bars, 10 µm. (C) IC-induced actin depolymerization. Polymerized actin was quantitated using a fluorometric phalloidin-binding assay. The ratio of FITC-phalloidin to DAPI intensity was expressed as the percentage of WT BMM without IC (n = 6). (D) IC-induced ERK phosphorylation. BMM were exposed to IC at 4°C for 20 min, washed, and incubated at 37°C for the times indicated. ERK and pERK were detected by Western blotting. (E) IC-induced change in PIP_2 homeostasis. BMM were challenged with or without IC for 2 min at 37°C. The PIP_2 level was quantitated by HPLC and expressed as the percentage of WT BMM without IC treatment (n = 3). Error bars indicate SEM.

alone had no effect. These results suggest that the shuttled PIP_2 can replenish the pool depleted by PIP5K-γ knockout and that the phenotypic changes are caused by a decrease in PIP_2 generated by PIP5K-γ rather than a loss of PIP5K-γ protein or its scaffolding function by itself.

Next we explored the relation between excessive actin polymerization and decreased particle attachment. Latrunculin B (Latr B), which depolymerizes actin filaments, restored particle attachment to *PIP5K*-γ−/− BMM at 0.05–0.2 µM but had a minimal effect on WT BMM (Fig. 3 C). At 0.5 µM, Latr B inhibited binding to WT BMM and was unable to rescue particle binding in *PIP5K*-γ−/− BMM (Fig. 3 C). Therefore, some actin polymerization is required for particle attachment, but too much inhibits it. A biphasic requirement for polymerized actin has been described previously in regulated exocytosis (Muallem et al., 1995).

We also used jasplakinolide (Jasp) to block dynamic actin remodeling in WT BMM. Jasp inhibited particle binding (Fig. 3 D), IC clustering (Fig. 3 E), and ERK activation (Fig. 3 F). Because Jasp treatment of WT BMM recapitulated multiple *PIP5K*-γ−/− BMM's defects and low-dose Latr B rescued them in knockout

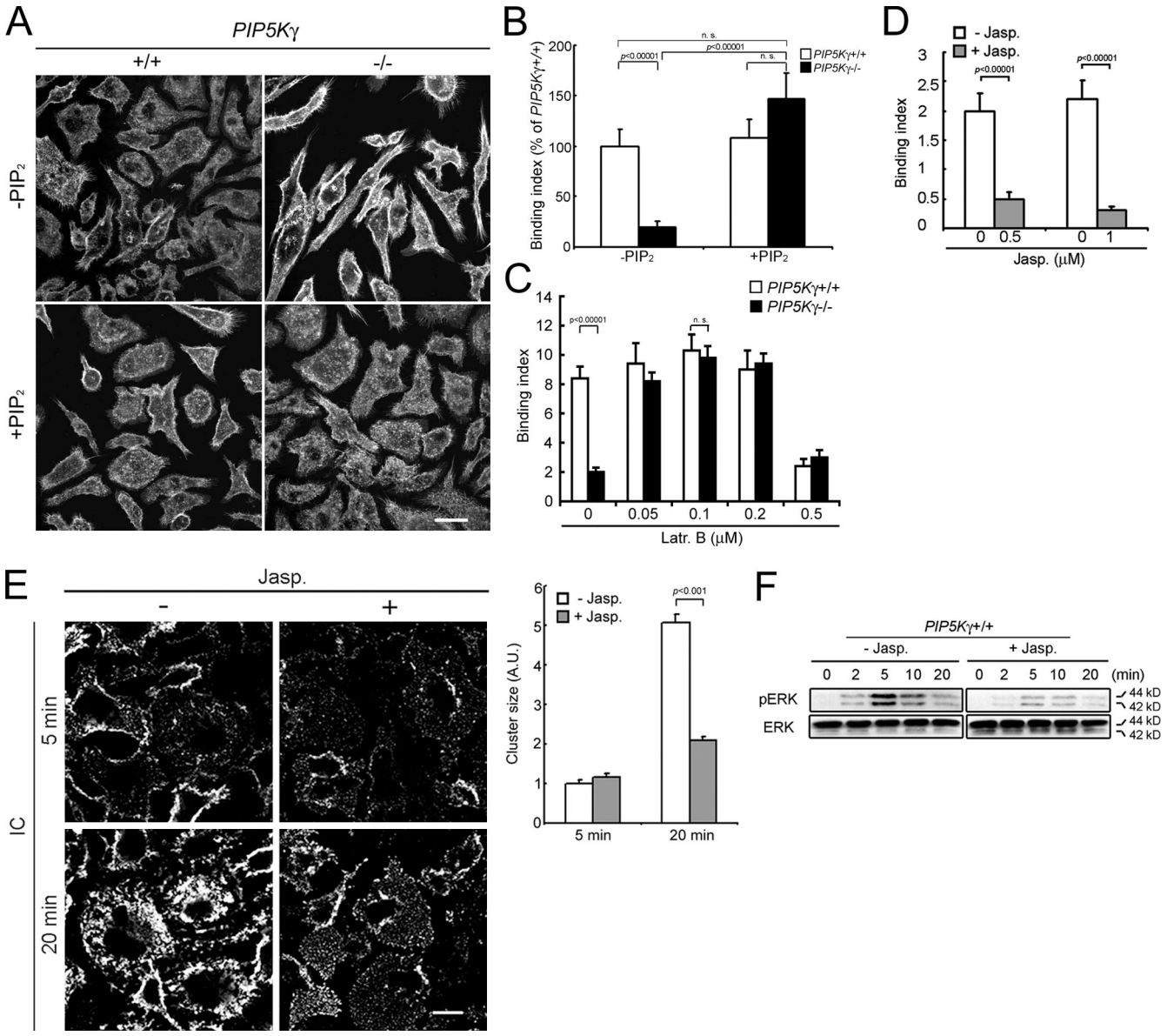

Figure 3. **The relation between *PIP5K*-γ deficiency, actin, particle attachment, and FcγR clustering defects.** (A) Rescue of cell shape and actin by PIP_2 shuttling. BMM with or without exogenously added PIP_2 were stained with phalloidin. (B) Rescue of particle attachment by PIP_2 delivery. Binding indices (n > 100) are expressed as the percentage of WT BMM without PIP_2. (C) Rescue of particle attachment by Latr B. Cells were incubated with Latr B for 5 min at 37°C before incubation with particles at 4°C (n > 70). (D) Inhibition of particle attachment to WT BMM by Jasp. Cells were incubated with 1 μM Jasp at 37°C for 30 min before the addition of IgG beads (n > 50). (E) Inhibition of FcγR clustering in WT BMM by Jasp. (left) Fluorescence staining of FcγR–IC clusters. (right) Cluster size quantitation (n > 1,000). Error bars indicate SEM. (F) Attenuation of IC-induced ERK phosphorylation by Jasp. Cells pretreated with or without Jasp were incubated with IC at 4°C for 20 min and warmed to 37°C. Bars, 10 μm.

cells, we conclude that controlled actin depolymerization facilitates FcγR microclustering, particle attachment, and signal amplification, and that PIP5K-γ generates the PIP_2 pool that regulates this depolymerization.

PIP5K-γ−/− BMM have abnormal Rac and Rho activation

Actin remodeling is regulated by a balance between the activation states of Rac and Rho GTPases (Burridge and Wennerberg, 2004). The *PIP5K*-γ−/− actin phenotype could be explained by an alteration in GTPase activation or their downstream effector functions. To distinguish between these possibilities, we determined if *PIP5K*-γ−/− knockdown disrupts Rac/Rho activation. GTPase effector pull-down assays showed that *PIP5K*-γ−/− BMM had a sixfold increase in GTP-RhoA and a 70% decrease in GTP-Rac1 (Fig. 4 A). Thus, PIP5K-γ knockout altered RhoA and Rac1 activation in opposite directions to tip the balance toward RhoA domination.

To examine the relation between abnormal Rho/Rac activation and cytoskeletal and phagocytic defects, we manipulated the intracellular content of activated GTPases using multiple approaches. RhoA was inhibited by the cell-permeable C3 transferase (C3T). In WT BMM, C3T had no effect on binding at 5 μg/ml but inhibited it at 10 μg/ml (Fig. 4 B). Thus, some

RhoA activity is required for normal particle attachment in WT cells. In contrast, C3T induced a dose-dependent increase in particle attachment to *PIP5K*-γ−/− BMM and converted them from an extended stellate to a more "normal" polygonal shape (Fig. 4 B). Therefore, excessive RhoA activation in *PIP5K*-γ−/− BMM inhibits actin remodeling and contributes to their particle attachment and morphological defects.

Rac1 is the major Rac isoform in BMM (Wells et al., 2004; Wheeler et al., 2006), and it is activated during the early stages of cup formation and extension (for review see Swanson, 2008). Tat-based protein transduction was used to introduce constitutively active Rac1L61 and dominant-negative (DN) Rac1N17 (Tskvitaria-Fuller et al., 2007). Rac1L61 converted the abnormally elongated *PIP5K*-γ−/− BMM to a more normal polygonal shape,

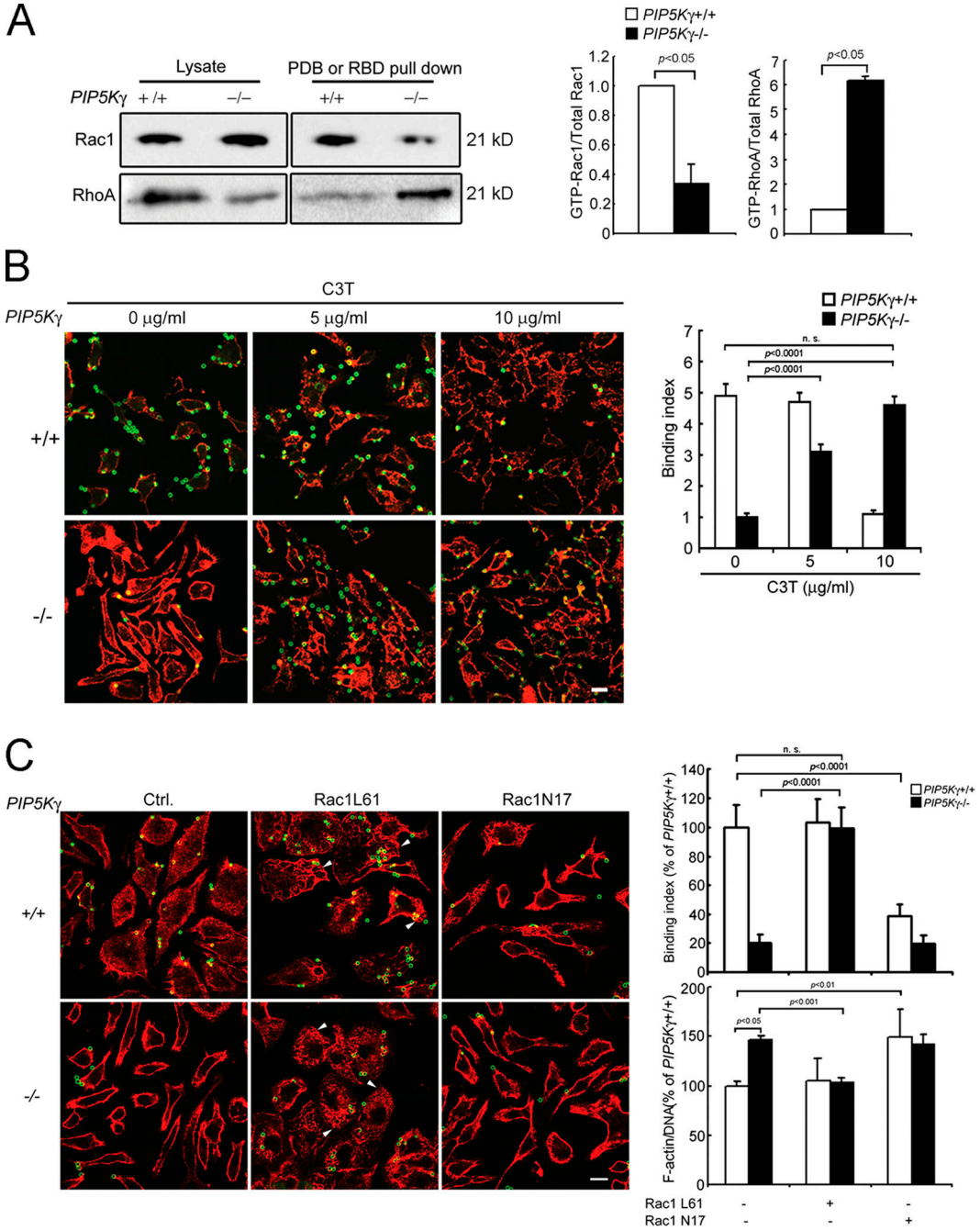

Figure 4. ***PIP5K*-γ−/− BMM have abnormal RhoA and Rac1 activation.** (A) GTP-Rac1 or -RhoA pull down by GST-PBD or -RBD, respectively. Samples were blotted with anti-Rac1 or -RhoA. (left) Western blot. Three times more WT BMM lysate and GST-RBD pull-down sample were loaded than *PIP5K*-γ−/− BMM. (right) Ratios of GTP-bound to total GTPase, expressed relative to the levels of WT BMM (n = 4 for Rac1 and 2 for RhoA). (B) Rescue of particle binding defect by C3T. BMM were incubated with C3T at 37°C for 4 h before the exposure of IgG-opsonized particles at 4°C. (left) Fluorescence staining. Green, external beads; red, phalloidin. (right) Binding indices (n > 70). (C) Effects of manipulating Rac activation. BMM were transduced with 600 nM Tat-Rac1L61 or N17 at 37°C for 30 min. (left) Fluorescence images. Green, external beads; red, phalloidin. Arrowheads indicate dorsal ruffles. (top right) Particle binding indices (n > 50). (bottom right) Fluorometric phalloidin quantitation (n = 3). Data are expressed as the percentage of WT BMM without transduced Rac1. Error bars indicate SEM. Bars, 10 μm.

restored particle binding, and decreased the amount of polymerized actin (Fig. 4 C). It also induced the formation of dorsal ruffles in WT and *PIP5K*-γ−/− BMM (Fig. 4 C, arrowheads). Rac1N17 had no obvious effect on *PIP5K*-γ−/− BMM, presumably because their endogenous Rac was already depressed in the absence of PIP5K-γ. However, Rac1N17 induced cell elongation, increased F-actin, and decreased particle binding in WT BMM to recapitulate the *PIP5K*-γ−/− phenotypes (Fig. 4 C). The reciprocal effects on *PIP5K*-γ−/− and WT BMM strongly suggest that Rac1 is necessary for particle attachment and that an imbalance of Rac1/RhoA contributes to *PIP5K*-γ−/− BMM's particle attachment and morphological defects. The finding that inhibiting RhoA or increasing Rac1 activity is sufficient to rescue *PIP5K*-γ−/− defects places PIP5K-γ upstream of RhoA/Rac1. This possibility has not been considered previously, as PIP5Ks are generally thought to be downstream effectors of Rho GTPases (for reviews see Yin and Janmey, 2003; Oude Weernink et al., 2004b; Mao and Yin, 2007).

PIP5K-α−/− BMM are defective in particle ingestion

We have recently generated a *PIP5K*-α−/− mouse line (human isoform designation; equivalent to mouse PIP5K-β; Wang et al., 2008a). The *PIP5K*-α−/− BMM did not express PIP5K-α (Fig. 5 A) but had normal total and surface FcγR (Fig. 5, A and B). TLC analysis showed that there was a small (∼20%) but statistically significant decrease in [^{32}P]PIP_2. HPLC analysis confirmed that the PIP_2 level was also decreased (Fig. 5 C). Western blotting showed that there was no compensatory change of PIP5K-γ (Fig. S1 B), which is consistent with findings in *PIP5K*-α−/− platelets (Wang et al., 2008a).

PIP5K-α−/− BMM had no obvious change in cell shape or phalloidin actin staining (Fig. 5 E). Fluorometric phalloidin quantitation confirmed that they had close to normal polymerized actin content (Fig. 5 D). In addition, they bound IgG-opsonized particles (Fig. 5 E) and phosphorylated ERK normally (Fig. 5 F). Nevertheless, they had a 60% decrease in ingestion index compared with WT BMM (Fig. 5 E). Thus, PIP5K-α has a different role in phagocytosis than PIP5K-γ.

PIP5K-α−/− BMM have impaired actin polymerization during ingestion

Particle ingestion is orchestrated by actin cytoskeletal changes during phagocytic cup initiation, cup extension, membrane closure, and phagosome pinching off from the PM (Swanson, 2008).

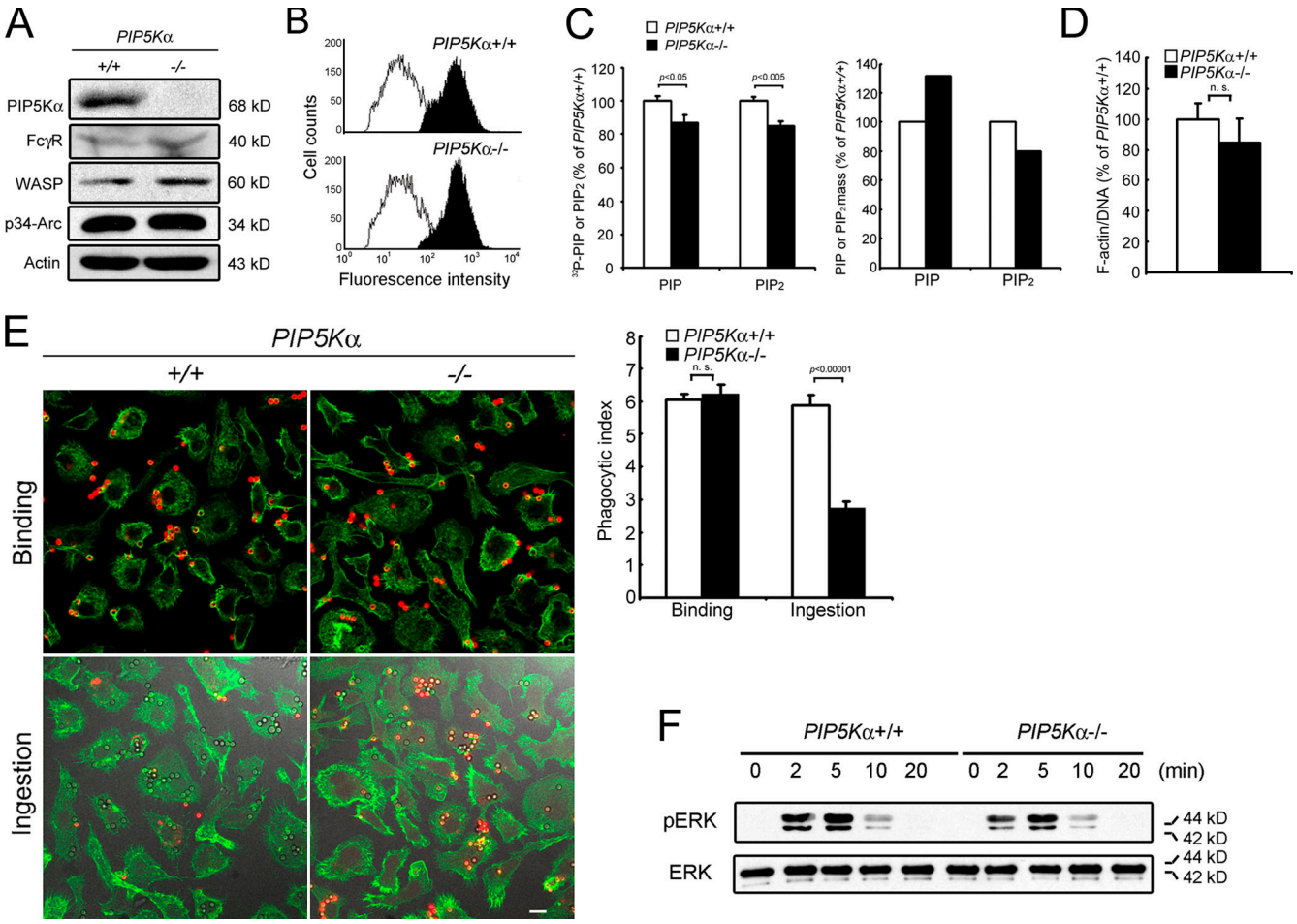

Figure 5. ***PIP5K*-α−/− BMM bind particles normally but ingest poorly.** (A) Western blot. (B) FACs analysis of surface-accessible FcγR. (C) Phosphoinositide profiles. (left) TLC (n = 3). (right) HPLC from a representative experiment from two independent determinations. (D) Fluorometric phalloidin quantitation (n = 4). (E) Particle attachment and ingestion. (left) Fluorescence/DIC images. Red, external beads; green, phallodin. (right) Phagocytic indices (n = ∼70). Bar, 10 µm. (F) IC-induced ERK phosphorylation. Error bars indicate SEM.

Actin and PIP_2 are enriched in the nascent phagocytic cup and in the advancing pseudopodia during cup extension (Scott et al., 2005). We used immunofluorescence microscopy to determine if PIP5K-α knockout impaired actin accumulation at the phagocytic cups. A line scan of the fluorescent-phalloidin intensity from the base of the cup (x) to the contralateral PM (y) showed that there was a twofold and 1.2-fold enrichment (x/y ratio) in the cups in WT and *PIP5K*-α−/− BMM, respectively. Thus, although *PIP5K*-α−/− BMM were able to initiate cup formation, their cups were shallower and were less efficient in mounting an actin polymerization response.

We performed additional studies to determine if WASP-mediated activation of the Arp2/3 complex was compromised. WASP is required for efficient phagocytosis (Lorenzi et al., 2000; May et al., 2000), and it is activated coordinately by PIP_2 and Cdc42 (Rohatgi et al., 1999). Overexpression of PIP5K promotes WASP and Arp2/3-dependent actin polymerization (Rozelle et al., 2000). Using a WASP antibody that recognizes the active open conformation (Labno et al., 2003), we found that there was no detectible staining in the cytoplasm of WT BMM but strong staining in the cups (Fig. 6 B). However, the antibody that detects total WASP stained both the cups and cytoplasm (Fig. 6 B, inset). Consistent with WASP activation in the cups, p34-Arc, a component of the Arp2/3 complex that binds active WASP, also accumulated there (Fig. 6 C).

In contrast, only ∼1% of the phagocytic cups in *PIP5K*-α−/− BMM had active WASP (Fig. 6 B) or p34-Arc staining (Fig. 6 C), although the knockout cells expressed normal amounts of WASP and Arp2/3 (Fig. 5 A), and WASP by itself was found in the cups (Fig. 6 B, inset). We conclude that WASP is recruited to the phagocytic cup independently of PIP5K-α but that WASP activation is highly dependent on PIP5K-α. Our results are in agreement with previous findings that WASP recruitment is not absolutely PIP_2 dependent per se (for review see Takenawa and Suetsugu, 2007) and establish PIP5K-α as the primary source of PIP_2 for WASP activation in the cup.

PIP5K-γ and -α depletion by RNAi

Our results from null mice provided definitive evidence for the differential roles of PIP5K-γ and -α in actin remodeling after long-term knockout. We next used RNAi to determine if depletion in the short term in another type of phagocytic cell has similar effects. Because BMM are difficult to transfect, we used the engineered phagocytic CHO-IIA cells, which stably express human FcγRIIA and phagocytize IgG-opsonized particles using a similar (albeit simpler) machinery (Downey et al., 1999). Compared with BMM, CHO-IIA cells had more PIP5K-α than PIP5K-γ (Fig. 1 A). PIP5K knockdown was confirmed by Western blotting (Fig. 7 A). As in knockout BMM, PIP5K-α depletion decreased the PIP_2 level in CHO-IIA cells to a larger extent than PIP5K-γ depletion (Fig. 7 B).

The PIP5K-depleted CHO-IIA cells exhibited phenotypic defects similar to those described above for the knockout BMM. PIP5K-γ knockdown decreased particle attachment, ingestion, and FcγRIIA microclustering, whereas PIP5K-α knockdown decreased ingestion but had no effect on attachment or microclustering (Figs. 7 C and S3, available at http://www.jcb.org/cgi/content/full/jcb.200806121/DC1). Like *PIP5K*-α−/− BMM, PIP5K-α–depleted CHO-IIA cells form nascent phagocytic cups that had less polymerized actin and less Arp2/3 enrichment (Figs. 7 D and S4 A), even though N-WASP (the WASP equivalent in nonhematopoietic cells) was present (Fig. S4 B).

In control CHO-IIA cells, endogenous PIP5K-α and the transfected PIP_2 reporter, EGFP-PLCδ1 pleckstrin homology domain (PH), were both enriched in the phagocytic cup (Fig. 7 E, arrowheads), as shown previously (Coppolino et al., 2002). After PIP5K-α depletion, there was no detectible PIP5K-α in the cup. EGFP-PLCδ1PH was associated with the attached particles, but its intensity was similar to that on the PM outside of the cups (Fig. 7 E). Therefore, PIP5K-α is primarily responsible for the large focal increase in PIP_2 during cup formation. PIP5K-γ was not able to contribute to this PIP_2 pool.

PIP5K-γ but not -α is tyrosine phosphorylated by Syk during phagocytosis

The differential roles of PIP5K-γ and -α can be most simply explained by their differential recruitment to phagocytic cup. However, immunofluorescence localization studies did not support this possibility. Within the limits of the resolution of our current approach, we found that both PIP5Ks were enriched in the nascent phagocytic cup and remained associated with the cup until completion of ingestion (Fig. 8 A). The conundrum of how these isoforms can exert independent and opposite control over the actin cytoskeleton in a sequential manner within the same restricted membrane region suggests that PIP5Ks may be subject to additional regulation.

FcγR ligation activates Src family and Syk tyrosine kinases in tandem to initiate the phagocytic signaling cascade (for reviews see Cox and Greenberg, 2001; Nimmerjahn and Ravetch, 2008). PIP5K-γ87 and -90 were both tyrosine phosphorylated when COS-IIA cells were stimulated with IgG- but not BSA-opsonized particles (Fig. 8 B). Phosphorylation peaked within 1–2 min and decreased thereafter. PIP5K-β was also tyrosine phosphorylated, but its phosphorylation peaked slightly later. In contrast, PIP5K-α was not detectibly tyrosine phosphorylated. Thus, PIP5Ks are differentially regulated, and transient PIP5K-γ tyrosine phosphorylation offers a potential explanation for the temporal regulation of its activity during phagocytosis. Because BMM and the engineered phagocytic cells (CHO-IIA and COS-IIA) have much more PIP5K-γ87 than PIP5K-90, we will focus on PIP5K-γ87 phosphorylation here.

Using a panel of tyrosine kinase inhibitors, we found that PIP5K-γ87 tyrosine phosphorylation was blocked by the Src inhibitor PP2 (not depicted) and the Syk inhibitor piceatannol (Fig. 8 C). Because Syk acts downstream of Src, we focused on the possibility that Syk is PIP5K-γ87's immediate physiological regulator. Syk is particularly abundant in hematopoietic cells and is also found in many other types of cells, including COS cells (Miah et al., 2004). We used a DN Syk to block endogenous Syk in COS-IIA and found that it inhibited IgG-induced increase in PIP5K-γ87 tyrosine phosphorylation (Fig. 8 D). In addition, Syk phosphorylated PIP5K-γ87 in vitro, and phosphorylation was blocked by piceatannol (Fig. 8 E). Unexpectedly, although PIP5K-α was not tyrosine phosphorylated in cells, it was phosphorylated by Syk in vitro (Fig. 8 E). This paradoxical result

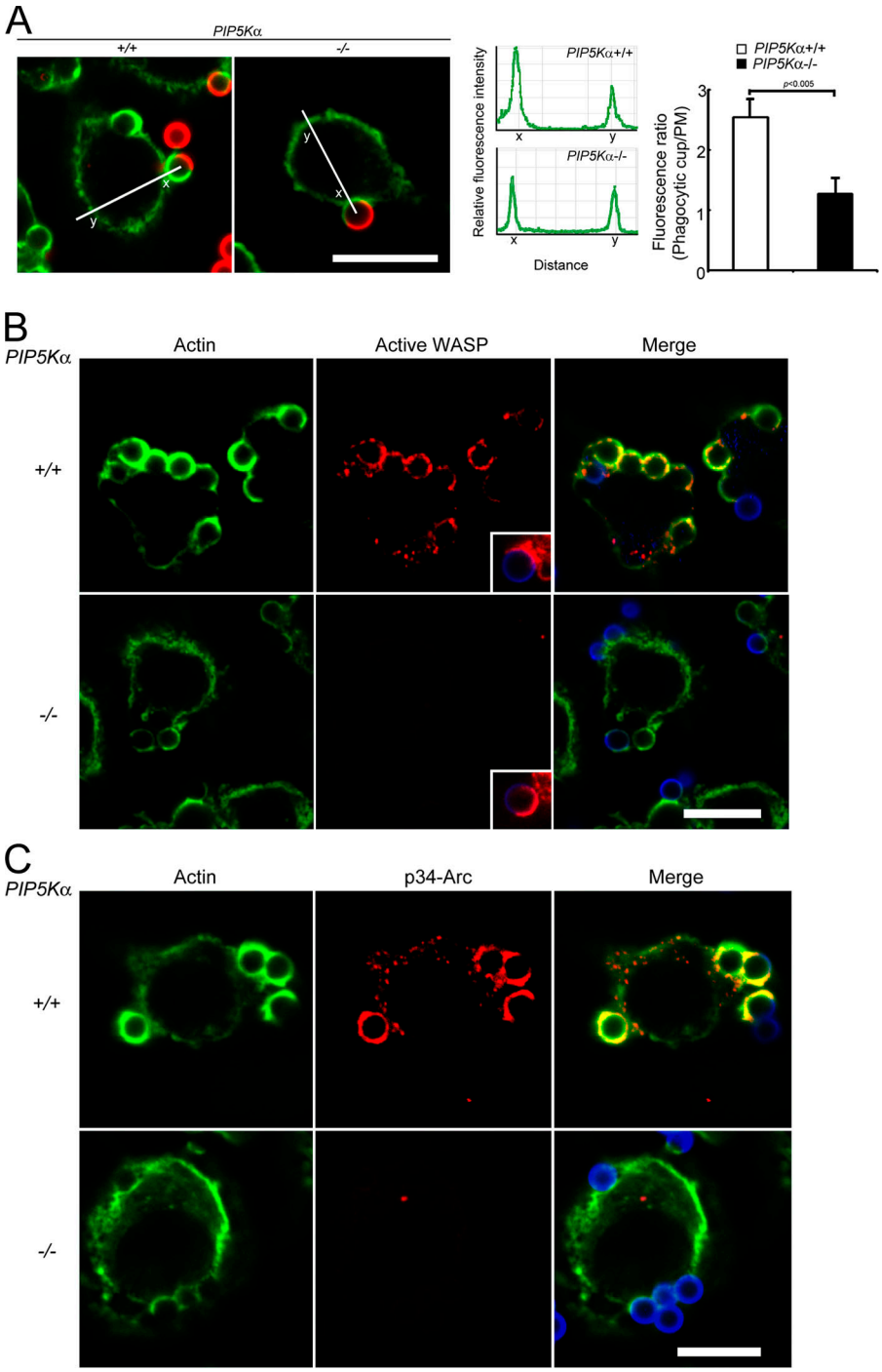

Figure 6. ***PIP5K*-α−/− BMM are defective in actin polymerization during ingestion.** BMM incubated with IgG-opsonized beads at 4°C for 10 min were warmed to 37°C for 1 min. (A) Quantitation of polymerized actin in situ. (left) Fluorescence images. Green, phalloidin; red, external beads. (middle) Line scans of phalloidin fluorescence intensity spanning the bottom of a nascent phagocytic cup (x) and its contralateral PM (y). Data shown were taken from representative cells. (right) Ratio of phalloidin intensity (x/y; n = 30 cups). Error bars indicate SEM. (B) Red, active WASP; green, phalloidin; blue, external beads. (inset) Total WASP (red) in another cell. (C) p34-Arc (red). Bars, 10 µm.

raises the intriguing possibility that PIP5K-α, unlike PIP5K-γ, may not be accessible to Syk in the intact cell.

We used an in vitro lipid kinase assay to examine the effect of tyrosine phosphorylation on PIP5K-γ87's catalytic activity. Pervanadate (PV), a potent tyrosine phosphatase inhibitor, was used to maximize tyrosine phosphorylation. Under conditions in which the rate of PIP_2 generation was linear, PIP5K-γ87 from PV-treated cells had a 2.3-fold higher specific activity than that from untreated cells (Fig. 8 F). Collectively, these results established that PIP5K-γ is activated by Syk-mediated phosphorylation during phagocytosis.

Discussion

PIP_2 regulates multiple biological processes at the PM (for reviews see Yin and Janmey, 2003; Di Paolo and De Camilli, 2006), and there is emerging evidence for the existence of functionally and/or spatially distinct PIP_2 pools contributed by different PIP5K isoforms (for review see Mao and Yin, 2007). The prevailing hypothesis is that these PIP5Ks are differentially recruited to membrane sites by binding isoform-specific adaptors. For example, PIP5K-γ90 is recruited to focal adhesions by binding talin through its unique 26–amino acid C-terminal

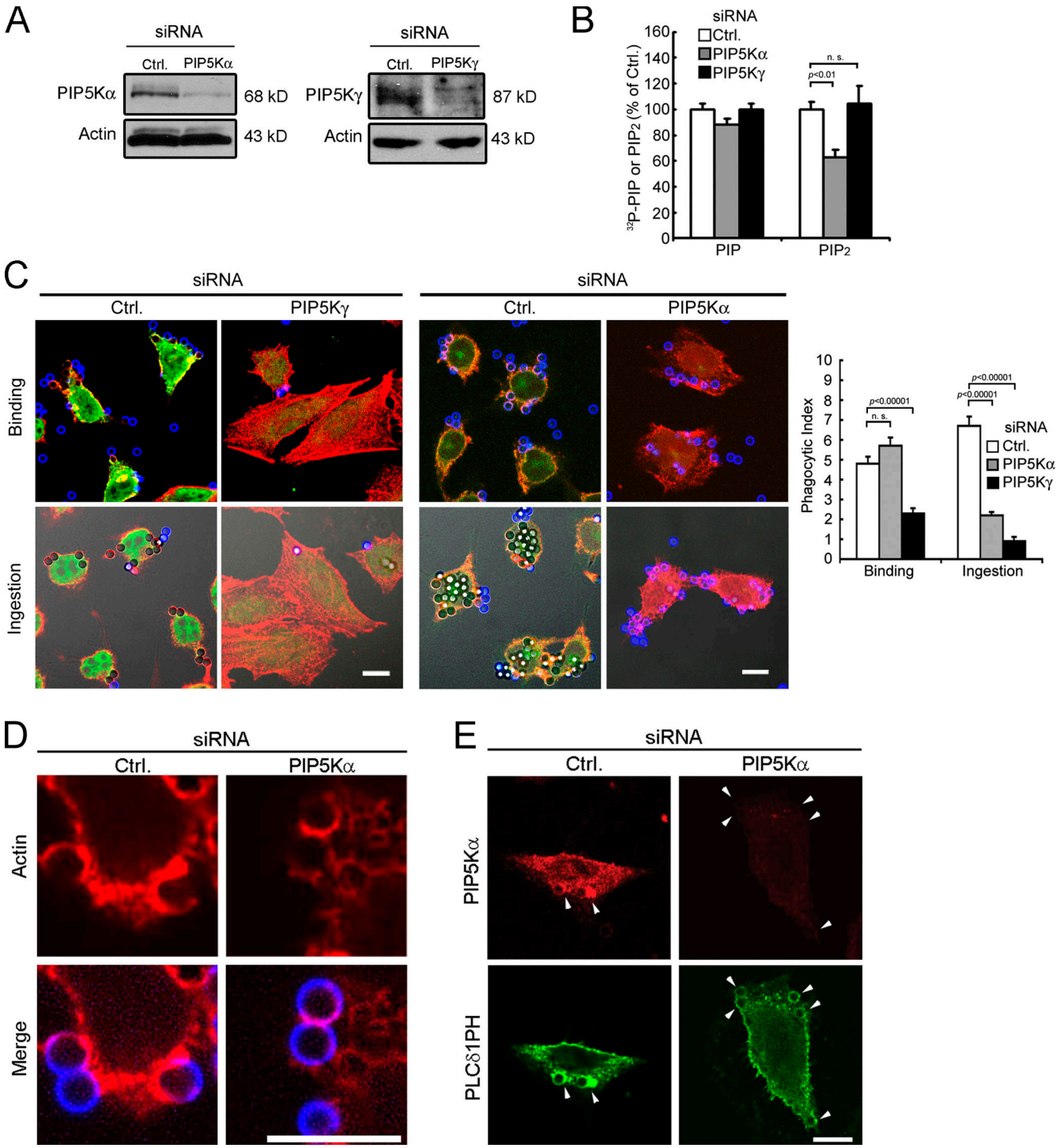

Figure 7. **PIP5K-γ and -α depletion by RNAi in CHO-IIA cells.** (A) Western blot. The amount of lysate used for PIP5K-γ detection was five times higher than that for other proteins because of its low abundance. (B) TLC analysis ($n = 5$). (C) Particle attachment and ingestion. (left) Fluorescence/DIC images. Green, PIP5K; blue, external beads; red, phalloidin. (right) Phagocytic indices ($n > 40$). (D and E) Cells with prebound beads were incubated at 37°C for 5 min. Error bars indicate SEM. (D) Phalloidin staining. Blue, external beads; red, phalloidin. (E) Endogenous PIP5K-α (red) and EGFP-PLCδ1PH (green). Arrowheads highlight phagocytic cups and particles being ingested. Bars, 10 μm.

extension, whereas PIP5K-γ87, which lacks the C-terminal tail, is not (Di Paolo et al., 2002; Ling et al., 2002). In addition, PIP5K-α is recruited to membrane ruffles by binding to Ajuba, a LIM protein (Kisseleva et al., 2005).

Here, we examined the role of PIP5K-γ and -α in phagocytosis. We chose this model because it is orchestrated by temporally distinct steps that are dependent on dynamic changes in actin and PIP_2 within the confines of the phagocytic cup (for reviews see Yeung et al., 2006; Swanson, 2008). PIP5K-γ and -α are both recruited to the phagocytic cup and remain there until phagosome closure. We show that the temporal segregation of the processes they regulate, despite their apparent coexistence

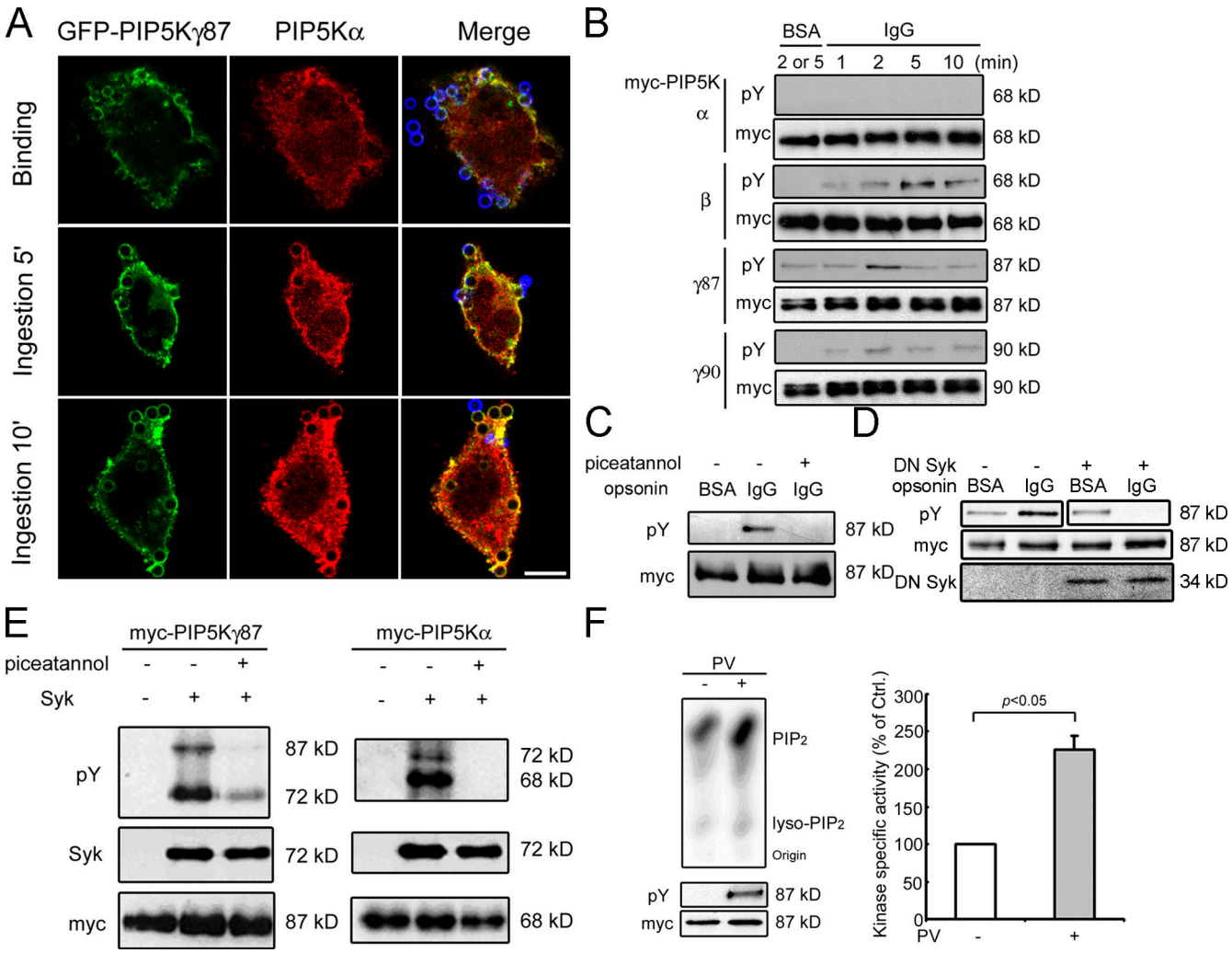

Figure 8. **PIP5K-γ87 regulation by Syk.** (A) Colocalization of PIP5K-γ87 and -α in CHO-IIA cells. Blue, external beads; red, endogenous PIP5K-α; green, overexpressed GFP–PIP5K-γ87. Bar, 10 µm. (B) Time course of PIP5K tyrosine phosphorylation. COS-IIA cells transfected with myc-PIP5K were challenged with BSA- or IgG-opsonized beads at 37°C for different amounts of time. PIP5Ks were immunoprecipitated and Western blotted. (C) Effect of piceatannol. Myc–PIP5K-γ87–transfected COS-IIA cells were treated with or without 50 µM piceatannol for 30 min and challenged with BSA- or IgG-opsonized beads at 37°C for 2 min. Immunoprecipitated myc–PIP5K-γ87 was immunoblotted. (D) The effect of DN Syk on myc–PIP5K-γ87 tyrosine phosphorylation. (E) In vitro tyrosine phosphorylation. Separately immunoprecipitated Syk and myc-PIP5Ks were incubated together with ATP. Phosphorylation was detected with anti-pY. (F) In vitro lipid kinase activity. Myc–PIP5K-γ87 immunoprecipitated from PV-treated COS cells were used for in vitro kinase assays. (left) Autoradiogram of ^{32}P-labeled PIP_2 products after TLC (top) and Western blotting of immunoprecipitated PIP5K-γ87 (bottom). (right) Kinase-specific activity (the amount of [^{32}P]PIP_2 generated in the linear portion of the kinase assay normalized against anti-myc intensity). The value from samples exposed to PV was expressed as the percentage of those without PV (n = 3). Error bars indicate SEM.

within the phagocytic cup, can be explained by their opposite effects on the actin cytoskeleton, their different placement within the small GTPase activation cascade, and their differential regulation by Syk. Our findings identify many novel aspects about the complex chain of events during phagocytosis and provide new insights into understanding other complex and dynamic PIP_2-dependent membrane processes.

PIP5K knockout mice

PIP5K-γ knockout, which is embryonically (Wang et al., 2007) or perinatally (Di Paolo et al., 2004) lethal, induces severe neurological and cardiac development abnormalities. We cannot explain why these two lines of knockout mice die at different stages, but note that both have significant actin cytoskeletal defects (Di Paolo et al., 2004; Wang et al., 2008b). Unlike the *PIP5K*-γ−/− mice, the *PIP5K*-α−/− mice have an implantation defect, but the occasional embryos that "escape" survive to adulthood (Wang et al., 2008a). We used PIP5K-γ−/− and -α−/− BMM here and did not examine the role of PIP5K-β, as BMM and CHO-IIA cells have very little PIP5K-β and we were not able to obtain the PIP5K-β knockout mice (Sasaki et al., 2005). Notably, *PIP5K-β*−/− mice are viable, have no fertility defects, and live a normal lifespan. The different effects of PIP5K knockout on mouse survival are consistent with their different in vivo roles.

PIP5K-γ and -α regulate different steps in phagocytosis

PIP5K-γ knockout or RNAi increases the amount of polymerized actin under basal conditions and decreases the cytoskeleton's

ability to depolymerize in response to FcγR ligation. These results support the actin "fence" model, which proposes that the subplasmalemmal actin meshwork tethers transmembrane receptors to restrict their lateral diffusion (Kusumi et al., 2005). In this scenario, excessive actin polymerization, coupled with the inability to depolymerize in response to FcγR ligation, impedes FcγR microclustering. Because other immunoreceptor tyrosine-based activation motif (ITAM) receptors, including T and B cell antigen receptors and mast cell Fcε receptors, also form microclusters (Villalba et al., 2001; Hao and August, 2005; Gupta et al., 2006; Kaizuka et al., 2007; Andrews et al., 2008), we suggest that the initial actin depolymerization phase associated with their clustering may also be regulated by PIP5K-γ. Because PIP5K-γ87 is so much more abundant than PIP5K-γ90 in BMM and CHO-IIA cells, we assume that most of the phenotypic changes described here are due primarily to the loss of PIP5K-γ87. Additional experiments will be required to sort out the individual contributions of each PIP5K-γ isoform.

PIP5K-α knockout or RNAi had no effect on particle binding but inhibited particle ingestion. WASP was recruited to the phagocytic cups but was not activated. Therefore, PIP5K-α promotes WASP activation and WASP-dependent de novo actin polymerization during particle ingestion. We speculate that actin polymerization during ingestion is facilitated by the abundant supply of actin monomers generated by PIP5K-γ during the initial attachment phase. However, because PIP5K-α and -γ have opposite effects on actin polymerization, PIP5K-γ has to be tuned down in order for PIP5K-α to achieve net polymerization. We hypothesize that this is achieved through PIP5K-γ dephosphorylation.

PIP5Ks are differentially regulated by tyrosine phosphorylation

PIP5Ks have been implicated in many cellular functions, but there is surprisingly little information about how they are regulated by tyrosine phosphorylation. Up until now, only PIP5K-γ90 (Ling et al., 2003) and PIP5K-β (Halstead et al., 2006) were known to be tyrosine phosphorylated, and there was no information about how any PIP5K isoform responds to FcγR ligation. Here, we show for the first time that PIP5K-γ87 is tyrosine phosphorylated and identify Syk, an apical master regulator of the phagocytic signaling cascade, as the immediate physiological regulator of PIP5K-γ87 during phagocytosis. PIP5K-γ regulation by Syk may provide cells with an elaborate positive feed-forward signaling network at the particle-binding stage. Significantly, because PIP5K-γ87 is transiently phosphorylated, this will generate a spike of PIP_2 to drive actin depolymerization during receptor ligation, and PIP5K-γ87 subsequently dialed down to allow PIP5K-α–initiated actin polymerization to dominate during particle engulfment.

We do not know at present if PIP5K-α activity is modulated during phagocytosis. Unlike PIP5K-γ, PIP5K-α is not tyrosine phosphorylated in cells, even though it can be phosphorylated by Syk in vitro. Because PIP5K-α and -γ coexist in the nascent phagocytic cup, this would imply that Syk may have differential access to these PIP5Ks. Because FcγR microclusters are recruited into Src-containing raft microdomains, and the Src-phosphorylated FcγR recruits Syk (Kwiatkowska et al., 2003; Garcia-Garcia et al., 2007), we speculate that PIP5K-γ, but not PIP5K-α, is also preferentially recruited to raft microdomains. The regulation of PIP5K-γ87 activity by tyrosine phosphorylation may also explain why even though BMM have abundant PIP5K-γ87, PIP5K-γ knockout does not decrease the amount of PIP_2 significantly. Perhaps PIP5K-γ87 is not maximally active under ambient conditions. Full activation may require its recruitment to the PM as well as tyrosine phosphorylation.

Relations between Rac1, RhoA and PIP5Ks

Rac promotes de novo actin polymerization during internalization (Swanson, 2008). Rho, which increases stress fibers in fibroblasts, has been implicated in the regulation of FcγR-mediated phagocytosis by some (Hackam et al., 1997; Hall et al., 2006) but not other studies (Caron and Hall, 1998; Olazabal et al., 2002). Recently, Hall et al. (2006) found that high-dose C3T significantly inhibits FcγR-mediated phagocytosis by an as-yet identified mechanism that is not mediated through the actin cytoskeleton. We find that extensive Rho inhibition or actin depolymerization inhibits particle attachment, establishing definitively that Rho does regulate FcγR-mediated phagocytosis; low-level Rho activity is required to maintain a minimal level of actin polymerization to induce FcγR microclustering, whereas too much Rho inhibits it.

Our results show that Rac1 and RhoA have reciprocal roles in the particle attachment step, as they do in other processes (Burridge and Wennerberg, 2004). *PIP5K*-γ−/− BMM have less GTP-Rac1 and more GTP-RhoA, and their phagocytic defects are rescued by inhibiting RhoA with C3T or by transducing the constitutively active Rac1L61. Because rescue occurs in the absence of PIP5K-γ, we conclude that PIP5K-γ acts upstream of Rac and Rho. This placement is different from previous models based on the assumption that PIP5Ks act exclusively downstream of these GTPases (for reviews see Yin and Janmey, 2003; Oude Weernink et al., 2004b; Mao and Yin, 2007). The prevailing model is based on the following findings: first, PIP5Ks bind Rho GTPases in GST pull-down assays, although binding is not dependent on GTPase activation (Ren et al., 1996; Oude Weernink et al., 2004a); and second, Rho GTPases increase PIP5K membrane recruitment and, in some cases, activity (Ren et al., 1996; Tolias et al., 1998; Chatah and Abrams, 2001). Our placement of PIP5K-γ upstream of Rho/Rac activation does not preclude its additional regulation by GTPases further downstream (Fig. 9). Also, based on previously published results, and PIP5K-α's role in WASP activation, we place PIP5K-α downstream of Rac/Cdc42 activation.

Additional experiments will be required to determine how PIP5K-γ regulates Rac/Rho activation. We speculate that it may activate Rac1 and suppress RhoA by altering the balance between their respective guanine nucleotide exchange factors, GTPase-activating proteins, and guanine nucleotide dissociation inhibitors. These may include inactivation of p190RhoGAP and activation of the RacGEF DOCK180 that have been implicated in phagocytosis (Continolo et al., 2005; Lee et al., 2007). There is a recent example of an interplay between PIP5K-β and a RhoGDI to activate RhoA (Lacalle et al., 2007).

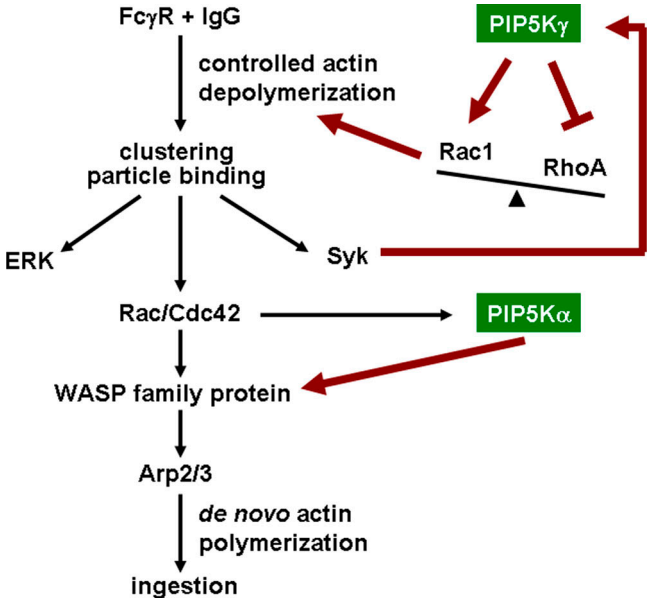

Figure 9. **Model for the unique roles and differential regulations of PIP5K-γ and -α in FcγR-mediated phagocytosis.** Controlled actin depolymerization is initiated upon FcγR ligation to IgG. PIP5K-γ activates Rac and inhibits Rho, tilting the balance toward actin disassembly. Actin remodeling releases the "tethering" of FcγR to promote formation of FcγR microclusters, which promote particle binding and downstream signaling including ERK and Syk activation. Syk further phosphorylates and activates PIP5K-γ in a positive feed-forward manner. PIP5K-α generates PIP_2 at the nascent phagocytic cup to activate WASP family proteins. Arp2/3 binds activated WASP and initiates de novo actin polymerization for particle ingestion. Our model places PIP5K-γ upstream of Rac/Rho based on data presented here, and places PIP5K-α downstream of Rac/Cdc42 based on previous published results and PIP5K-α's role in WASP activation described here. Our model does not preclude additional feedback regulation of PIP5K-γ by these small GTPases.

Our model for the differential roles of PIP5Ks during phagocytosis

To summarize, we have established a role of PIP5K-γ in maintaining the balance between Rac/Rho activation and in dynamic remodeling of the actin cytoskeleton to promote FcγR clustering, particle attachment, and signal propagation. We show that the *PIP5K*-γ−/− phenotype is caused by the loss of the PIP5K-γ–generated PIP_2 pool. We have also established a role of PIP5K-α in activating WASP to induce de novo actin polymerization in the phagocytic cup. We propose the following working model (Fig. 9). Under basal conditions, PIP5K-γ maintains a dynamic actin cytoskeleton. FcγR binding to IgG recruits PIP5K-γ to the site of particle attachment. PIP5K-γ initiates controlled actin depolymerization by tilting the Rho family GTPase balance toward increased Rac activation. Dynamic actin remodeling releases the "tethering" of FcγR by the subplasmalemmal actin cytoskeleton to facilitate receptor oligomerization. Receptor microclustering robustly activates Syk, which further activates PIP5K-γ by tyrosine phosphorylation in a positive feed-forward manner. The overall effect is an increase in the avidity of FcγR for IgG to promote stable particle attachment and signal amplification. This stages the attachment site for the subsequent ingestion step by generating an abundant supply of actin monomers to fuel de novo actin polymerization. PIP5K-γ is tuned down by dephosphorylation, and PIP5K-α generates PIP_2 at the nascent phagocytic cup to recruit Arp2/3 by activating WASP. Unlike PIP5K-γ, PIP5K-α is likely to act primarily downstream of Rac/Cdc42 and it is not phosphorylated by Syk.

Materials and methods

Antibodies, cDNA constructs, and reagents

All chemicals and reagents were obtained from Sigma-Aldrich unless otherwise indicated. Other materials included: recombinant CSF-1 (R&D Systems); polyclonal anti–PIP5K-γpan and –PIP5K-γ90 (Wenk et al., 2001); anti–PIP5K-β (a gift from C.L. Carpenter, Harvard Medical School, Boston, MA; Yang et al., 2004); anti–PIP5K-α, -RhoA, -ERK, -Syk, -myc, -WASP, and -pY (Santa Cruz Biotechnology, Inc.); anti–active WASP (a gift from M.K. Rosen, University of Texas Southwestern Medical Center, Dallas, TX; Labno et al., 2003); anti-Rac1, –N-WASP and –p34-Arc (Millipore); phycoerythrin–anti-CD45.1, FITC–anti-CD45.2, allophycocyanin (APC)–anti-CD4, and anti-FcγRIIB/III mAb 2.4G2 (BD Biosciences); anti-pERK (Cell Signaling Technology); anti-actin (Millipore); fluorescent-conjugated secondary antibodies (Jackson ImmunoResearch Laboratories); HRP-conjugated secondary antibodies (GE Healthcare); [^{32}P]PO_4 and [γ-^{32}P]ATP (PerkinElmer); C3T (Cytoskeleton, Inc.); Jasp and piceatannol (EMD); and Latr B (Invitrogen). Epitope-tagged PIP5Ks were as described previously (Padron et al., 2003). Human Syk and DN Syk (Syk SH2 domain only, aa 1–261) were cloned into the pCMV5 vector (Bonnerot et al., 1998).

Bone marrow transplantation and BMM differentiation in vitro

PIP5K-γ−/− mice were generated by breeding *PIP5K*-γ+/− mice (Di Paolo et al., 2004). Liver cells isolated from newborn *PIP5K*-γ−/− or +/+ pups (C57BL/6J CD45.2) were injected into lethally irradiated WT adult recipient mice (C57BL/6J CD45.1). The genotypes of the newborn donor mice used for transplantation were established by PCR analysis of genomic DNA isolated from mouse heads. Reconstitution in the chimera was confirmed by FACs analysis. Bone marrow progenitor cells were isolated 3–9 mo after transplantation. *PIP5K*-α−/− mice (human isoform designation, even when referring to knockout in mice) were generated by breeding *PIP5K*-α+/− mice (Wang et al., 2008a) and used directly for bone marrow isolation. *PIP5K*-α+/+ mice from the same litter were used as WT controls. Bone marrow progenitor cells were cultured in macrophage differentiation medium (DME containing 30% L929-conditional medium, 1% [vol/vol] MEM vitamins, and 1% [vol/vol] penicillin/streptomycin; Hall et al., 2006) and used for experiments after 5–10 d in culture.

Flow cytometry

Determining reconstitution efficiency. Spleen cells collected from chimeric mice were simultaneously stained with PE–anti-CD45.1, FITC–anti-CD45.2, and allophycocyanin (APC)–anti-CD4, and sorted by FACSCalibur (BD). CD4+ cells were gated and their CD45.1/CD45.2 profiles were determined.

Determining the amount of FcγR on the BMM cell surface. BMM were fixed and suspended at 2.5 × 10^7 cells/ml in PBS containing 3% BSA. Cells were incubated with 2.4G2 (1:50) at RT for 60 min, stained with Alexa Fluor 488–conjugated goat anti–rat IgG (1:200) for 30 min at RT, and subjected to FACScan analysis. Autofluorescence was determined in cells without 2.4G2 staining. Data were analyzed using CellQuest software (BD).

Quantitative RT-PCR

Total RNA was extracted and reverse transcribed to generate cDNA for PCR in an ABI Prism 7000 sequence detection system (Applied Biosystems). The mRNA level of PIP5K was determined by comparing its mean threshold cycle to that of cyclophilin. Primers used were: cyclophilin forward, 5′-TGGAGAGCACCAAGACAGACA-3′, and reverse, 5′-TGCCGGAGTCGACAATGAT-3′; PIP5K-α forward, 5′-AGAAGTTGGAGCACTCTTGG-3′, and reverse, 5′-GAGAAGGCTTCAAGGGAATC-3′; PIP5K-β forward, 5′-AGGAGATCGTATCCTCCATC-3′, and reverse, 5′-AATGATGGAGTGCTGGGTAC-3′; PIP5K-γpan forward, 5′-TGTTGCCTTCCGCTACTTC-3′, and reverse, 5′-GGCTCATTGCACAGGGAGTAC-3′; and PIP5K-γ90 forward, 5′-AGCCTCTGTGGAAATAGACGCT-3′, and reverse, 5′-GAGTACACCCAGCTCCTCTCGT-3′.

Immunofluorescence microscopy

For most experiments, cells were fixed with 3.7% formaldehyde, permeabilized with 0.1% Triton X-100, and processed for confocal microscopy. In some cases, cells were fixed but not permeabilized before staining to detect epitopes on the cell surface. Images were collected by a 63×/ 1.4NA

Plan Apo oil-immersion objective on a laser scanning confocal microscope (Axiovert 100M) using LSM 510 Meta software (all from Carl Zeiss, Inc.).

Phosphoinositide measurements

TLC. ^{32}P incorporation into PIP and PIP_2 was determined by labeling cells for 4 h with 35 µCi/ml [^{32}P]PO_4 in phosphate-free DME (Invitrogen; Yamamoto et al., 2006). Lipids were extracted, resolved by TLC, detected by autoradiography, and analyzed by ImageQuant TL software (GE Healthcare). The amount of [^{32}P]PIP_2 or PIP was expressed as a percentage of ^{32}P incorporation into total phospholipids in the autoradiogram.

HPLC. Lipid mass was determined and normalized against total lipids eluted as described previously (Yamamoto et al., 2001).

Phagocytosis assays

Latex particles were opsonized with 1 mg/ml human IgG (1 h at 37°C or overnight at 4°C; Coppolino et al., 2002). In most cases, 3-µm beads were used, except for in Fig. 8, in which 1-µm beads were used to increase the extent of stimulation for phosphorylation experiments. Particles in serum-free medium were allowed to attach to cells for 10–15 min at 4°C and washed extensively (binding). For ingestion, cells in warm serum-free medium were incubated for 5 min (for BMM, unless otherwise indicated) or 15 min (for CHO-IIA cells, unless otherwise indicated) at 37°C. Externally accessible beads were detected by labeling fixed but not permeabilized cells with anti–human IgG for 10 min. Proteins inside cells were stained after permeabilization of the fixed cells. Differential interference contrast (DIC) microscopy was used to visualize beads (external and internal), and confocal laser microscopy was used to visualize fluorescently labeled proteins. The number of beads on the cell surface or inside the cells was counted in 5–10 randomly chosen fields (with ~30–50 cells per field) and expressed as the binding or ingestion index (mean number of beads per cell), respectively.

IC-induced FcγR clustering

Heat-aggregated IC (100 µg/ml final), prepared as previously described (Sobota et al., 2005), were incubated with cells for 5 or 20 min at 4°C. FcγR–IgG complexes were visualized by staining fixed cells with anti-IgG or 2.4G2. The size of the clusters in immunofluorescence images was analyzed with ImageJ software in multiple randomly chosen fields.

Fluorometric phalloidin actin quantitation

Phalloidin binding to fixed and permeabilized BMM was quantitated fluorometrically (Cox et al., 1996). BMM attached to a 24-well plate were fixed, permeabilized, and stained with 0.35 µM FITC-phalloidin and 10 µg/ml DAPI. Samples were excited at 360/480 nm, and emissions at 460/530 nm were recorded by FL600 microplate fluorescence reader (BioTek). F-actin content per cell was defined as the ratio of FITC to DAPI fluorescence intensity, after subtracting background autofluorescence.

PIP_2 shuttling

Carrier 3 and diC16-PIP_2 (both from Echelon Biosciences) were premixed at an equal molar ratio (each at 100 µM) at RT for 10 min and added to BMM at a final concentration of 10 µM (Wang et al., 2003). After a 10-min incubation at 37°C, the medium was replaced with serum-free medium containing particles for binding assays. Control cells were incubated with shuttle carrier without PIP_2.

GTP-Rac and -Rho effector pull-down assays

BMM were lysed in a buffer containing 25 mM Hepes, pH 7.5, 150 mM NaCl, 10 mM $MgCl_2$, 1 mM EDTA, 10% glycerol, 1% NP-40, and protease inhibitors. Clarified lysates were incubated with either GST-PAK-PBD or GST-Rhotekin-RBD immobilized on glutathione–Sepharose 4B beads (Cytoskeleton Inc.) for 45 min at 4°C. Rac1 and RhoA contents were determined by Western blotting.

Tat-Rac1 protein transduction

The HA-tagged Tat-Rac1L61 (constitutively active) and Tat-Rac1N17 (DN) constructs were gifts of C. Wulfing (University of Texas Southwestern Medical Center, Dallas, TX). Recombinant Tat fusion proteins were purified under nonreducing conditions (Tskvitaria-Fuller et al., 2007) and added to BMM suspended at 2 × 10^6 cells/ml in polyhema-coated 6-well plates for 30 min at 37°C. Cells were washed and seeded onto coverslips or 24-well plates, and the attached cells were used after 10 min at 37°C.

RNAi

CHO-IIA cells (a gift from S. Grinstein, Hospital for Sick Children, Toronto, Ontario, Canada) that stably expressed human FcγRIIA were maintained in DME containing 10% FBS and 0.5 mg/ml G418. They were seeded at a density of 5 × 10^4 cells per 12-mm glass coverslip and transfected with siRNA using Oligofectamine (Invitrogen). Cells were used 48 later. Hamster PIP5K sequences were obtained by cloning using primers from conserved human/mouse sequences (PIP5K-α forward, 5′-GCTGCAGAGCTTCAAGAT-3′, and reverse, 5′-GAACTCTGACTCTGCAAC-3′; and PIP5K-γ forward, 5′-AAGCCACCACAGCCTCCAT-3′, and reverse, 5′-TTATGTGTCGCTCTCGCC-3′). The siRNA used were 5′-AAATCAGTGAAGGCTCACCTG-3′ and 5′-ATCATCAAGACCGTCATGCAC-3′ for PIP5K-α and -γ, respectively. An oligonucleotide (5′-AAGAATATTGTTGCAC-3′) that targets firefly luciferase was used as a control.

In vitro PIP5K phosphorylation by Syk

COS cells were separately transfected with myc-PIP5K and Syk using Lipofectamine 2000 (Invitrogen). Cells were lysed, and myc-PIP5K or Syk was immunoprecipitated with anti-myc or -Syk and protein G–Sepharose beads. Beads were resuspended in kinase buffer (50 mM Hepes, pH 7.4, 10 mM $MgCl_2$, 10 mM $MnCl_2$, and 10 µM sodium vanadate) in the presence or absence of piceatannol. ATP was added to a final concentration of 2 µM and in vitro phosphorylation was terminated after 20 min at RT. Tyrosine phosphorylation was detected by Western blotting with anti-pY.

In vitro lipid kinase assay

COS cells were transfected with myc–PIP5K-γ87. 24 h later, cells were treated for 10 min with or without 2 mM PV freshly prepared from orthovanadate and hydrogen peroxide (Rozelle et al., 2000). Myc–PIP5K-γ87 was immunoprecipitated with anti-myc/protein G–Sepharose beads. The beads were suspended in a solution containing 50 mM Tris-HCl, pH 7.4, 100 mM NaCl, 15 mM $MgCl_2$, 1 mM EGTA, 0.4 mg/ml BSA, 250 mM sucrose, 0.4% polyethylene glycol 20,000, 0.04% Triton X-100, 80 µM PI4P, and 80 µM phosphatidylserine (Avanti Polar Lipids, Inc.; Yamamoto et al., 2001). [γ-^{32}P]ATP was added (1 µCi/50 µl, 50 µM final) and phosphorylation was terminated after 10 min at RT. Lipids were separated by TLC and quantified with a Phosphorimager (GE Healthcare) analysis. Equivalent immunoprecipitates were Western blotted by anti-myc and -pY. Specific lipid kinase activity was obtained by normalizing ^{32}P-PIP_2 to the amount of immunoprecipitated myc–PIP5K-γ87, as determined by Western blotting.

Statistical analysis

All data were expressed as mean ± SEM, and the two-tailed unpaired *t* test was used to analyze the statistical significance.

Online supplemental material

Fig. S1 shows the reconstitution efficiency in chimeric mice and confirms that there was no compensatory increase of PIP5K-α in *PIP5K-γ−/−* BMM, and vice versa. Fig. S2 compares the use of anti-IgG versus anti-FcγR to quantitate IC-induced microclustering. Fig. S3 shows that IC-induced FcγRIIA microclustering was defective in PIP5K-γ but not -α RNAi cells. Fig. S4 shows that the recruitment of p34-Arc but not N-WASP to the phagocytic cup was impaired in PIP5K-α–depleted cells. Online supplemental material is available at http://www.jcb.org/cgi/content/full/jcb.200806121/DC1.

We thank colleagues at University of Texas Southwestern Medical Center for their contributions: C. Wulfing (Tat-Rac1 constructs and purification protocols), D.H. Hilgemann (HPLC analysis), and M.K. Rosen (anti-active WASP antibody). We also thank C.L. Carpenter (Harvard Medical School) for anti–PIP5K-β antibody, J.S. Brugge (Harvard Medical School) for BMM culture protocols, and S. Grinstein (Hospital for Sick Children at Toronto) for the COS- and CHO-IIA cell lines.

This work was supported by grants from the National Institutes of Health (P50-GM21681 Burn Center Grant and R01-GM06110 to H.L. Yin, R01-NS056049 to G. Di Paolo, R01-CA03922-24 to M. Bennett, R01-HL083392 and PO1-HL40387 to C.S. Abrams, and R01-DK069633 to C.Y. Lu) and by the Robert A. Welch Foundation (grant I-1200 to H.L. Yin).

Submitted: 20 June 2008
Accepted: 22 December 2008

References

Andrews, N.L., K.A. Lidke, J.R. Pfeiffer, A.R. Burns, B.S. Wilson, J.M. Oliver, and D.S. Lidke. 2008. Actin restricts FcepsilonRI diffusion and facilitates antigen-induced receptor immobilization. *Nat. Cell Biol.* 10:955–963.

Bonnerot, C., V. Briken, V. Brachet, D. Lankar, S. Cassard, B. Jabri, and S. Amigorena. 1998. syk protein tyrosine kinase regulates Fc receptor gamma-chain-mediated transport to lysosomes. *EMBO J.* 17:4606–4616.

Botelho, R.J., M. Teruel, R. Dierckman, R. Anderson, A. Wells, J.D. York, T. Meyer, and S. Grinstein. 2000. Localized biphasic changes in phosphatidylinositol-4,5-bisphosphate at sites of phagocytosis. *J. Cell Biol.* 151:1353–1368.

Burridge, K., and K. Wennerberg. 2004. Rho and Rac take center stage. *Cell.* 116:167–179.

Caron, E., and A. Hall. 1998. Identification of two distinct mechanisms of phagocytosis controlled by different Rho GTPases. *Science.* 282:1717–1721.

Chatah, N.E., and C.S. Abrams. 2001. G-protein-coupled receptor activation induces the membrane translocation and activation of phosphatidylinositol-4-phosphate 5-kinase I alpha by a Rac- and Rho-dependent pathway. *J. Biol. Chem.* 276:34059–34065.

Continolo, S., A. Baruzzi, M. Majeed, E. Caveggion, L. Fumagalli, C.A. Lowell, and G. Berton. 2005. The proto-oncogene Fgr regulates cell migration and this requires its plasma membrane localization. *Exp. Cell Res.* 302:253–269.

Coppolino, M.G., R. Dierckman, J. Loijens, R.F. Collins, M. Pouladi, J. Jongstra-Bilen, A.D. Schreiber, W.S. Trimble, R. Anderson, and S. Grinstein. 2002. Inhibition of phosphatidylinositol-4-phosphate 5-kinase Ialpha impairs localized actin remodeling and suppresses phagocytosis. *J. Biol. Chem.* 277:43849–43857.

Corbett-Nelson, E.F., D. Mason, J.G. Marshall, Y. Collette, and S. Grinstein. 2006. Signaling-dependent immobilization of acylated proteins in the inner monolayer of the plasma membrane. *J. Cell Biol.* 174:255–265.

Cox, D., and S. Greenberg. 2001. Phagocytic signaling strategies: Fc(gamma)receptor-mediated phagocytosis as a model system. *Semin. Immunol.* 13:339–345.

Cox, D., P. Chang, T. Kurosaki, and S. Greenberg. 1996. Syk tyrosine kinase is required for immunoreceptor tyrosine activation motif-dependent actin assembly. *J. Biol. Chem.* 271:16597–16602.

Di Paolo, G., and P. De Camilli. 2006. Phosphoinositides in cell regulation and membrane dynamics. *Nature.* 443:651–657.

Di Paolo, G., L. Pellegrini, K. Letinic, G. Cestra, R. Zoncu, S. Voronov, S. Chang, J. Guo, M.R. Wenk, and P. De Camilli. 2002. Recruitment and regulation of phosphatidylinositol phosphate kinase type 1 gamma by the FERM domain of talin. *Nature.* 420:85–89.

Di Paolo, G., H.S. Moskowitz, K. Gipson, M.R. Wenk, S. Voronov, M. Obayashi, R. Flavell, R.M. Fitzsimonds, T.A. Ryan, and P. De Camilli. 2004. Impaired PtdIns(4,5)P2 synthesis in nerve terminals produces defects in synaptic vesicle trafficking. *Nature.* 431:415–422.

Downey, G.P., R.J. Botelho, J.R. Butler, Y. Moltyaner, P. Chien, A.D. Schreiber, and S. Grinstein. 1999. Phagosomal maturation, acidification, and inhibition of bacterial growth in nonphagocytic cells transfected with FcgammaRIIA receptors. *J. Biol. Chem.* 274:28436–28444.

Garcia-Garcia, E., E.J. Brown, and C. Rosales. 2007. Transmembrane mutations to FcgammaRIIA alter its association with lipid rafts: implications for receptor signaling. *J. Immunol.* 178:3048–3058.

Griffin, F.M. Jr., and S.C. Silverstein. 1974. Segmental response of the macrophage plasma membrane to a phagocytic stimulus. *J. Exp. Med.* 139:323–336.

Groves, E., A.E. Dart, V. Covarelli, and E. Caron. 2008. Molecular mechanisms of phagocytic uptake in mammalian cells. *Cell. Mol. Life Sci.* 65:1957–1976.

Gupta, N., B. Wollscheid, J.D. Watts, B. Scheer, R. Aebersold, and A.L. DeFranco. 2006. Quantitative proteomic analysis of B cell lipid rafts reveals that ezrin regulates antigen receptor-mediated lipid raft dynamics. *Nat. Immunol.* 7:625–633.

Hackam, D.J., O.D. Rotstein, A. Schreiber, W. Zhang, and S. Grinstein. 1997. Rho is required for the initiation of calcium signaling and phagocytosis by Fcgamma receptors in macrophages. *J. Exp. Med.* 186:955–966.

Hall, A.B., M.A. Gakidis, M. Glogauer, J.L. Wilsbacher, S. Gao, W. Swat, and J.S. Brugge. 2006. Requirements for Vav guanine nucleotide exchange factors and Rho GTPases in FcgammaR- and complement-mediated phagocytosis. *Immunity.* 24:305–316.

Halstead, J.R., J. van Rheenen, M.H. Snel, S. Meeuws, S. Mohammed, C.S. D'Santos, A.J. Heck, K. Jalink, and N. Divecha. 2006. A role for PtdIns(4,5)P2 and PIP5Kalpha in regulating stress-induced apoptosis. *Curr. Biol.* 16:1850–1856.

Hao, S., and A. August. 2005. Actin depolymerization transduces the strength of B-cell receptor stimulation. *Mol. Biol. Cell.* 16:2275–2284.

Ishihara, H., Y. Shibasaki, N. Kizuki, T. Wada, Y. Yazaki, T. Asano, and Y. Oka. 1998. Type I phosphatidylinositol-4-phosphate 5-kinases. Cloning of the third isoform and deletion/substitution analysis of members of this novel lipid kinase family. *J. Biol. Chem.* 273:8741–8748.

Kaizuka, Y., A.D. Douglass, R. Varma, M.L. Dustin, and R.D. Vale. 2007. Mechanisms for segregating T cell receptor and adhesion molecules during immunological synapse formation in Jurkat T cells. *Proc. Natl. Acad. Sci. USA.* 104:20296–20301.

Kisseleva, M., Y. Feng, M. Ward, C. Song, R.A. Anderson, and G.D. Longmore. 2005. The LIM protein Ajuba regulates phosphatidylinositol 4,5-bisphosphate levels in migrating cells through an interaction with and activation of PIPKI alpha. *Mol. Cell. Biol.* 25:3956–3966.

Kusumi, A., C. Nakada, K. Ritchie, K. Murase, K. Suzuki, H. Murakoshi, R.S. Kasai, J. Kondo, and T. Fujiwara. 2005. Paradigm shift of the plasma membrane concept from the two-dimensional continuum fluid to the partitioned fluid: high-speed single-molecule tracking of membrane molecules. *Annu. Rev. Biophys. Biomol. Struct.* 34:351–378.

Kwiatkowska, K., J. Frey, and A. Sobota. 2003. Phosphorylation of FcgammaRIIA is required for the receptor-induced actin rearrangement and capping: the role of membrane rafts. *J. Cell Sci.* 116:537–550.

Labno, C.M., C.M. Lewis, D. You, D.W. Leung, A. Takesono, N. Kamberos, A. Seth, L.D. Finkelstein, M.K. Rosen, P.L. Schwartzberg, and J.K. Burkhardt. 2003. Itk functions to control actin polymerization at the immune synapse through localized activation of Cdc42 and WASP. *Curr. Biol.* 13:1619–1624.

Lacalle, R.A., R.M. Peregil, J.P. Albar, E. Merino, A.C. Martinez, I. Merida, and S. Manes. 2007. Type I phosphatidylinositol 4-phosphate 5-kinase controls neutrophil polarity and directional movement. *J. Cell Biol.* 179:1539–1553.

Lee, W.L., G. Cosio, K. Ireton, and S. Grinstein. 2007. Role of CrkII in Fcgamma receptor-mediated phagocytosis. *J. Biol. Chem.* 282:11135–11143.

Ling, K., R.L. Doughman, A.J. Firestone, M.W. Bunce, and R.A. Anderson. 2002. Type I gamma phosphatidylinositol phosphate kinase targets and regulates focal adhesions. *Nature.* 420:89–93.

Ling, K., R.L. Doughman, V.V. Iyer, A.J. Firestone, S.F. Bairstow, D.F. Mosher, M.D. Schaller, and R.A. Anderson. 2003. Tyrosine phosphorylation of type Igamma phosphatidylinositol phosphate kinase by Src regulates an integrin-talin switch. *J. Cell Biol.* 163:1339–1349.

Lorenzi, R., P.M. Brickell, D.R. Katz, C. Kinnon, and A.J. Thrasher. 2000. Wiskott-Aldrich syndrome protein is necessary for efficient IgG-mediated phagocytosis. *Blood.* 95:2943–2946.

Mao, Y.S., and H.L. Yin. 2007. Regulation of the actin cytoskeleton by phosphatidylinositol 4-phosphate 5 kinases. *Pflugers Arch.* 455:5–18.

May, R.C., E. Caron, A. Hall, and L.M. Machesky. 2000. Involvement of the Arp2/3 complex in phagocytosis mediated by FcgammaR or CR3. *Nat. Cell Biol.* 2:246–248.

Miah, S.M., K. Sada, P.T. Tuazon, J. Ling, K. Maeno, S. Kyo, X. Qu, Y. Tohyama, J.A. Traugh, and H. Yamamura. 2004. Activation of Syk protein tyrosine kinase in response to osmotic stress requires interaction with p21-activated protein kinase Pak2/gamma-PAK. *Mol. Cell. Biol.* 24:71–83.

Micucci, F., C. Capuano, E. Marchetti, M. Piccoli, L. Frati, A. Santoni, and R. Galandrini. 2008. PI5KI-dependent signals are critical regulators of the cytolytic secretory pathway. *Blood.* 111:4165–4172.

Muallem, S., K. Kwiatkowska, X. Xu, and H.L. Yin. 1995. Actin filament disassembly is a sufficient final trigger for exocytosis in nonexcitable cells. *J. Cell Biol.* 128:589–598.

Nakano-Kobayashi, A., M. Yamazaki, T. Unoki, T. Hongu, C. Murata, R. Taguchi, T. Katada, M.A. Frohman, T. Yokozeki, and Y. Kanaho. 2007. Role of activation of PIP5Kgamma661 by AP-2 complex in synaptic vesicle endocytosis. *EMBO J.* 26:1105–1116.

Nimmerjahn, F., and J.V. Ravetch. 2008. Fcgamma receptors as regulators of immune responses. *Nat. Rev. Immunol.* 8:34–47.

Olazabal, I.M., E. Caron, R.C. May, K. Schilling, D.A. Knecht, and L.M. Machesky. 2002. Rho-kinase and myosin-II control phagocytic cup formation during CR, but not FcgammaR, phagocytosis. *Curr. Biol.* 12:1413–1418.

Oude Weernink, P.A., K. Meletiadis, S. Hommeltenberg, M. Hinz, H. Ishihara, M. Schmidt, and K.H. Jakobs. 2004a. Activation of type I phosphatidylinositol 4-phosphate 5-kinase isoforms by the Rho GTPases, RhoA, Rac1, and Cdc42. *J. Biol. Chem.* 279:7840–7849.

Oude Weernink, P.A., M. Schmidt, and K.H. Jakobs. 2004b. Regulation and cellular roles of phosphoinositide 5-kinases. *Eur. J. Pharmacol.* 500:87–99.

Ozaki, S., D.B. DeWald, J.C. Shope, J. Chen, and G.D. Prestwich. 2000. Intracellular delivery of phosphoinositides and inositol phosphates using polyamine carriers. *Proc. Natl. Acad. Sci. USA.* 97:11286–11291.

Padron, D., Y.J. Wang, M. Yamamoto, H. Yin, and M.G. Roth. 2003. Phosphatidylinositol phosphate 5-kinase Iβ recruits AP-2 to the plasma membrane and regulates rates of constitutive endocytosis. *J. Cell Biol.* 162:693–701.

Ren, X.D., G.M. Bokoch, A. Traynor-Kaplan, G.H. Jenkins, R.A. Anderson, and M.A. Schwartz. 1996. Physical association of the small GTPase Rho with a 68-kDa phosphatidylinositol 4-phosphate 5-kinase in Swiss 3T3 cells. *Mol. Biol. Cell.* 7:435–442.

Rohatgi, R., L. Ma, H. Miki, M. Lopez, T. Kirchhausen, T. Takenawa, and M.W. Kirschner. 1999. The interaction between N-WASP and the Arp2/3 complex links Cdc42-dependent signals to actin assembly. *Cell.* 97:221–231.

Rozelle, A.L., L.M. Machesky, M. Yamamoto, M.H. Driessens, R.H. Insall, M.G. Roth, K. Luby-Phelps, G. Marriott, A. Hall, and H.L. Yin. 2000. Phosphatidylinositol 4,5-bisphosphate induces actin-based movement of raft-enriched vesicles through WASP-Arp2/3. *Curr. Biol.* 10:311–320.

Sasaki, J., T. Sasaki, M. Yamazaki, K. Matsuoka, C. Taya, H. Shitara, S. Takasuga, M. Nishio, K. Mizuno, T. Wada, et al. 2005. Regulation of anaphylactic responses by phosphatidylinositol phosphate kinase type I {alpha}. *J. Exp. Med.* 201:859–870.

Scott, C.C., W. Dobson, R.J. Botelho, N. Coady-Osberg, P. Chavrier, D.A. Knecht, C. Heath, P. Stahl, and S. Grinstein. 2005. Phosphatidylinositol-4,5-bisphosphate hydrolysis directs actin remodeling during phagocytosis. *J. Cell Biol.* 169:139–149.

Sobota, A., A. Strzelecka-Kiliszek, E. Gladkowska, K. Yoshida, K. Mrozinska, and K. Kwiatkowska. 2005. Binding of IgG-opsonized particles to Fc gamma R is an active stage of phagocytosis that involves receptor clustering and phosphorylation. *J. Immunol.* 175:4450–4457.

Swanson, J.A. 2008. Shaping cups into phagosomes and macropinosomes. *Nat. Rev. Mol. Cell Biol.* 9:639–649.

Takenawa, T., and S. Suetsugu. 2007. The WASP-WAVE protein network: connecting the membrane to the cytoskeleton. *Nat. Rev. Mol. Cell Biol.* 8:37–48.

Tolias, K.F., A.D. Couvillon, L.C. Cantley, and C.L. Carpenter. 1998. Characterization of a Rac1- and RhoGDI-associated lipid kinase signaling complex. *Mol. Cell. Biol.* 18:762–770.

Tskvitaria-Fuller, I., N. Mistry, S. Sun, and C. Wulfing. 2007. Protein transduction as a means of effective manipulation of Cdc42 activity in primary T cells. *J. Immunol. Methods.* 319:64–78.

Villalba, M., K. Bi, F. Rodriguez, Y. Tanaka, S. Schoenberger, and A. Altman. 2001. Vav1/Rac-dependent actin cytoskeleton reorganization is required for lipid raft clustering in T cells. *J. Cell Biol.* 155:331–338.

Wang, Y., L. Lian, J.A. Golden, E.E. Morrisey, and C.S. Abrams. 2007. PIP5KI gamma is required for cardiovascular and neuronal development. *Proc. Natl. Acad. Sci. USA.* 104:11748–11753.

Wang, Y., X. Chen, L. Lian, T. Tang, T.J. Stalker, T. Sasaki, L.F. Brass, J.K. Choi, J.H. Hartwig, and C.S. Abrams. 2008a. Loss of PIP5KIbeta demonstrates that PIP5KI isoform-specific PIP2 synthesis is required for IP3 formation. *Proc. Natl. Acad. Sci. USA.* 105:14064–14069.

Wang, Y., R.I. Litvinov, X. Chen, T.L. Bach, L. Lian, B.G. Petrich, S.J. Monkley, D.R. Critchley, T. Sasaki, M.J. Birnbaum, et al. 2008b. Loss of PIP5KIgamma, unlike other PIP5KI isoforms, impairs the integrity of the membrane cytoskeleton in murine megakaryocytes. *J. Clin. Invest.* 118:812–819.

Wang, Y.J., J. Wang, H.Q. Sun, M. Martinez, Y.X. Sun, E. Macia, T. Kirchhausen, J.P. Albanesi, M.G. Roth, and H.L. Yin. 2003. Phosphatidylinositol 4 phosphate regulates targeting of clathrin adaptor AP-1 complexes to the Golgi. *Cell.* 114:299–310.

Wang, Y.J., W.H. Li, J. Wang, K. Xu, P. Dong, X. Luo, and H.L. Yin. 2004. Critical role of PIP5KIγ87 in InsP3-mediated Ca(2+) signaling. *J. Cell Biol.* 167:1005–1010.

Wells, C.M., M. Walmsley, S. Ooi, V. Tybulewicz, and A.J. Ridley. 2004. Rac1-deficient macrophages exhibit defects in cell spreading and membrane ruffling but not migration. *J. Cell Sci.* 117:1259–1268.

Wenk, M.R., L. Pellegrini, V.A. Klenchin, G. Di Paolo, S. Chang, L. Daniell, M. Arioka, T.F. Martin, and P. De Camilli. 2001. PIP kinase Igamma is the major PI(4,5)P(2) synthesizing enzyme at the synapse. *Neuron.* 32:79–88.

Wheeler, A.P., C.M. Wells, S.D. Smith, F.M. Vega, R.B. Henderson, V.L. Tybulewicz, and A.J. Ridley. 2006. Rac1 and Rac2 regulate macrophage morphology but are not essential for migration. *J. Cell Sci.* 119:2749–2757.

Yamamoto, M., D.H. Hilgemann, S. Feng, H. Bito, H. Ishihara, Y. Shibasaki, and H.L. Yin. 2001. Phosphatidylinositol 4,5-bisphosphate induces actin stress-fiber formation and inhibits membrane ruffling in CV1 cells. *J. Cell Biol.* 152:867–876.

Yamamoto, M., M.Z. Chen, Y.J. Wang, H.Q. Sun, Y. Wei, M. Martinez, and H.L. Yin. 2006. Hypertonic stress increases phosphatidylinositol 4,5-bisphosphate levels by activating PIP5KIbeta. *J. Biol. Chem.* 281:32630–32638.

Yang, S.A., C.L. Carpenter, and C.S. Abrams. 2004. Rho and Rho-kinase mediate thrombin-induced phosphatidylinositol 4-phosphate 5-kinase trafficking in platelets. *J. Biol. Chem.* 279:42331–42336.

Yeung, T., B. Ozdamar, P. Paroutis, and S. Grinstein. 2006. Lipid metabolism and dynamics during phagocytosis. *Curr. Opin. Cell Biol.* 18:429–437.

Yin, H.L., and P.A. Janmey. 2003. Phosphoinositide regulation of the actin cytoskeleton. *Annu. Rev. Physiol.* 65:761–789.